NASA
Technical
Paper
2075

September 1982

Circumferentially Segmented Duct Liners Optimized for Axisymmetric and Standing-Wave Sources

Willie R. Watson

NASA

NASA
Technical
Paper
2075

1982

Circumferentially Segmented Duct Liners Optimized for Axisymmetric and Standing-Wave Sources

Willie R. Watson
Langley Research Center
Hampton, Virginia

National Aeronautics
and Space Administration

**Scientific and Technical
Information Branch**

INTRODUCTION

Rising energy costs as well as current and proposed noise regulations have prompted continuing research and development of lighter weight, improved noise-suppression systems for the turbofan engines of commercial aircraft. The use of uniform acoustic duct liners (liners with wall impedances that do not vary axially or circumferentially) to suppress the noise generated by these turbofan engines is well established. However, the above factors require that acoustic-liner designs be continually refined and updated to incorporate new concepts. Recently, variable-impedance liner concepts (fig. 1) have been considered in the design of more effective noise-suppression systems.

Literature on axially segmented liners, a concept initially derived by Zorumski (ref. 1), is exhaustive. Lester and Posey (ref. 2) have shown that an axially segmented liner with two sections gives more suppression than the best uniform liner. Sawdy, Beckemeyer, and Patterson (ref. 3) have shown that this increase in suppression is due to a scattering of the sound at the first axial discontinuity into higher order radial modes, which are then more highly damped by the second section. However, certain characteristics of axially segmented liners limit their usefulness. These include lack of a broadband attenuation spectrum and inability to outperform uniform liners for well cut-on modes (ref. 4).

Mani (ref. 5) observed experimentally that an additional suppression of as much as 5 dB could be obtained at some directivity angles by circumferentially segmenting a uniform liner. He suggested that the increased suppression was because of scattering of acoustic energy into higher order circumferential modes, which were more highly damped. In addition, Mani suggested combining axially and circumferentially segmented liners to form a checkerboard pattern. These experimental findings motivated researchers to develop analytical models to verify these findings. Thus, in this instance, duct-acoustics experimental work has preceded and guided analytical development in liner technology.

Development of reliable analytical models for predicting noise suppression in ducts with circumferentially segmented liners is a prerequisite to the optimum design of these liners. Watson (ref. 6) developed a no-flow model for a rectangular duct based on a finite-element method, while Astley et al. (ref. 7) incorporated the effects of a sheared mean flow into a circular duct using the finite-element method. Since the finite-element methods developed in references 6 and 7 are in core solutions, the number of circumferential strips is severely restricted and the effects of the sound source are difficult to evaluate. These models are therefore not suited for optimization studies. Namba and Fukushige (ref. 8) used the equivalent surface-source method to evaluate attenuation properties of circumferentially segmented liners in a rectangular duct with uniform mean flow. They concluded that circumferentially segmented acoustic liners bring about modal transfer of sound energy between modes of different circumferential wave numbers and lead to higher power attenuation levels and broader effective attenuation bandwidth than a uniform liner. Watson (ref. 9) used the Galerkin method (ref. 10) to evaluate attenuation properties in circular ducts without mean flow. Results indicated that circumferentially segmented liners scatter energy between circumferential modes of different orders and lead to broader attenuation curves. However, before circumferentially segmented liners can be fully evaluated, additional studies evaluating the effects of

frequency, source complexity, and duct length are needed. Such liners should also be optimally designed to achieve maximum suppression and their off-optimum properties should be explored before their potential benefit can be fully realized.

This paper assesses the relative merits of circumferentially segmented liners by comparing their optimum attenuation properties with those of optimized uniform liners. Off-optimum properties are also discussed as well as effects of frequency, source complexity, and duct length. The analytical prediction program developed in reference 9 is used in conjunction with an optimization method to compute optimum properties for the uniform and segmented liner. The optimization method uses the Davidon-Fletcher-Powell algorithm (ref. 11). However, a series of two-dimensional contour maps is used to obtain good starting values for the algorithm. Both plane and circumferential standing-wave sources are considered in the study. Finally, emphasis is placed on segmented-lining configurations consisting of hard-wall/soft-wall combinations of the kind considered by Mani (ref. 5).

ANALYSIS

Consider a semi-infinite circular duct with radius $\bar{a}$, as shown in figure 2. (A list of symbols used in this paper appears after the references.) A circumferentially segmented liner with specific acoustic admittance $\beta(\theta)$ is placed along the outer wall, and an initial noise source in terms of a pressure boundary condition is given at $\bar{z} = 0$. Further, the segmented liner is assumed to consist of two piecewise uniform liners with admittances β_1 and β_2, as shown in figure 3. These piecewise uniform liners are combined in circumferential series to form a total of $2T$ strips. The admittance function $\beta(\theta)$ is expanded as the Fourier series

$$\beta(\theta) = \beta_{av} + \frac{2(\beta_1 - \beta_2)}{\pi}\left(\sin T\theta + \frac{\sin 3T\theta}{3} + \frac{\sin 5T\theta}{5} + \ldots\right) \tag{1}$$

where β_{av} is the average value of $\beta(\theta)$ for the circumferentially segmented liner

$$\beta_{av} = \frac{1}{2\pi}\int_0^{2\pi} \beta(\theta)\, d\theta = \frac{\beta_1 + \beta_2}{2}$$

and T is the periodicity of the liner. Within the context of this paper an optimized circumferentially segmented liner is defined as a liner configuration possessing uniform admittance β_1 and β_2 chosen to maximize the transmission loss over the length L. Finding this optimized liner is the major thrust of this paper.

Dimensionless acoustic waves propagating within the duct depicted in figure 2 satisfy the Helmholtz equation (ref. 9)

$$\nabla^2 P(r,\theta,z) + K^2 P(r,\theta,z) = 0 \tag{2}$$

in which a time dependence of the form $e^{-i\overline{\omega}t}$ has been assumed, $K = \overline{\omega a}/\bar{c}$ is the wave number, P is the dimensionless acoustic pressure, $\bar{\omega}$ is the angular

frequency, ∇^2 is the Laplace operator, $\bar{t}$ denotes time, and $\bar{c}$ is the ambient speed of sound. Throughout this paper, all distances are referred to the duct radius $\bar{a}$ and the acoustic pressure is referred to the quantity $\bar{\rho}\bar{c}^2$, in which $\bar{\rho}$ is the ambient density of the medium. In addition, the boundary condition along the outer wall is expressed in terms of the admittance $\beta(\theta)$ as follows:

$$\frac{\partial P(1,\theta,z)}{\partial r} = iK\ \beta(\theta)\ P(1,\theta,z) \tag{3}$$

whereas the boundary condition at the source plane is expressed as follows:

$$P(r,\theta,0) = Q(r,\theta) \tag{4}$$

where $Q(r,\theta)$ is the known source pressure function.

Equations (2) to (4) constitute a boundary value problem for the acoustic pressure field $P(r,\theta,z)$. Furthermore, this field can only contain waves running to the right because the duct in figure 2 is semi-infinite. In this paper, the solution is obtained by the eigenfunction expansion technique (ref. 3). The eigenfunction expansion technique expands the acoustic pressure field in terms of the eigenfunctions of the circumferentially segmented liner:

$$P(r,\theta,z) = \sum_{\ell=0}^{\infty} A_\ell\ P_\ell(r,\theta)\ \exp(iK_\ell z) \tag{5}$$

in which K_ℓ is the complex axial wave number and $P_\ell(r,\theta)$ is the acoustic pressure eigenfunction for the circumferentially segmented liner. Solutions for the eigenfunction $P_\ell(r,\theta)$ and for the axial wave number are developed in the following section. These eigenfunctions can also be shown to be orthogonal (ref. 9), so that substituting equation (5) into equation (4) and making use of the orthogonality condition allows the following determination of A_ℓ:

$$A_\ell = \frac{\int_0^{2\pi}\int_0^1 Q(r,\theta)\ P_\ell(r,\theta)\ r\ dr\ d\theta}{\int_0^{2\pi}\int_0^1 P_\ell^2(r,\theta)\ r\ dr\ d\theta} \tag{6}$$

A measure of the liner effectiveness as a sound absorber is given by the transmission-loss function TL as

$$TL(\beta_1,\beta_2) = 10\ \log_{10}[W(0)/W(L)] \tag{7}$$

and

$$W(z) = \mathrm{Re}\left(\int_0^{2\pi}\int_0^1 iP^* \frac{\partial P}{\partial z}\, r\, dr\, d\theta\right) \tag{8}$$

where Re( ) denotes the real part of the complex expression within the parentheses and the superscript asterisk indicates the complex conjugate. The value of the transmission-loss function can be obtained once the solution for the eigenfunction and for the axial wave number is obtained. The methodology used to obtain these solutions is described in the following section.

Solution for Eigenfunction and Axial Wave Number

If equation (5) is substituted into equations (2) and (3), each eigenfunction $P_\ell(r,\theta)$ can be shown to satisfy a Helmholtz equation

$$\nabla^2 P_\ell(r,\theta) + \lambda_\ell^2 P_\ell(r,\theta) = 0 \tag{9}$$

with the homogeneous boundary conditions

$$\frac{\partial P_\ell(r,\theta)}{\partial r} - iK\,\beta(\theta)\,P_\ell(r,\theta) = 0 \qquad (r = 1) \tag{10}$$

where ∇^2 is the two-dimensional Laplace operator in r and θ and the eigenvalue λ_ℓ is related to the axial wave number by the equation

$$\lambda_\ell^2 = K^2 - K_\ell^2 \tag{11}$$

Equations (9) to (11) constitute an eigenvalue problem which must be solved to obtain the eigenfunction $P_\ell(r,\theta)$ and the axial wave number K_ℓ. An exact analytical solution to this eigenvalue problem is possible and is developed in appendix A. The analytical solution requires finding the roots of a transcendental equation which include Bessel functions of many orders. To avoid the complexity of iteratively solving this transcendental equation, a numerical solution to this eigenvalue problem is obtained. The methodology for obtaining this numerical solution is described in the following paragraphs.

The numerical technique for obtaining solutions to equations (9) and (10) is exactly as presented in reference 9 and only enough will be repeated to provide the

necessary nomenclature and ground work for the optimization method. Thus, the solution for the eigenfunction $P_\ell(r,\theta)$ is expressed in the form

$$P_\ell(r,\theta) = \sum_{m=0}^{M} \sum_{n=0}^{N} \left(A_{m,n}^{\ell} \cos m\theta + B_{m,n}^{\ell} \sin m\theta \right) \frac{J_m(\lambda_{m,n} r)}{N_{m,n}} \tag{12}$$

where $\lambda_{m,n}$ represents the hard-wall eigenvalues which satisfy the transcendental equation $J_m'(\lambda_{m,n}) = 0$ and the normalization constant $N_{m,n}$ is

$$N_{m,n}^2 = \int_0^{2\pi} \int_0^1 \cos^2 m\theta \, J_m^2(\lambda_{m,n} r) \, r \, dr \, d\theta$$

Galerkin's method allows determination of the modal coefficients $A_{m,n}^{\ell}$ and $B_{m,n}^{\ell}$ as well as the eigenvalue λ_ℓ.

There remains the problem of determining the number of circumferential and radial modes (M and N) which are needed in equation (12) to obtain an accurate resolution for the eigenmode $P_\ell(r,\theta)$. Strictly speaking, N should be determined such that the exact radial dependence of the exact eigenmode is accurately resolved by the series of hard-wall modes, or

$$J_m(\lambda_\ell r) = \sum_{n=0}^{N} d_n \, J_m(\lambda_{m,n} r)$$

where d_n is an appropriately chosen constant. Studies reported in reference 9, as well as additional ones performed by the author, show that $N = 9$ gives good agreement between the exact and the numerically computed mode shape for a range of frequencies and m numbers considered here. Thus, results in this paper will be computed with $N = 9$.

A simple rule of thumb for determining the upper index of summation M has been developed. This index should be chosen so that the incident wave can be accurately resolved by substituting $z = 0$ into equation (5). In addition, M is intimately related to the periodicity of the liner. For purposes of this paper, consideration is restricted to six circumferential modes. This does not mean that $M = 5$, since it is shown in appendix A that only selected values of m should appear in equation (12) for any spatially discrete given source. Thus, only the first six of these selected values of m are included. This particular choice of M was based on convergence studies in which it was observed that virtually no change in the transmission loss occurs as M is increased beyond this value for a range of frequencies and duct lengths.

Scattering From Two Axial Discontinuities

A finite-length circumferentially segmented liner combined with two semi-infinite hard-wall sections as depicted in figures 4 and 5 is now used for the study

of the problem of scattering from two axial discontinuities. An acoustic wave p^I from the left is incident at $z = 0$. This results in a reflected wave p^R in the first hard-wall section as well as a transmitted wave p^t in the second hard-wall section. It is necessary to compute the resulting transmission loss over the circumferentially segmented liner. In general, interaction of the incident wave with the peripheral liner is expected to result in modal transfer of acoustic energy among radial and circumferential modes of different orders.

The constant geometry of the present problem makes it amenable to the mode matching technique (ref. 3). Thus, the incident, reflected, and transmitted waves in the hard-wall sections are expressed in terms of hard-wall duct modes

$$p^I(r,\theta,z) = \sum_{m=0}^{M}\sum_{n=0}^{N}\left(a^I_{m,n}\cos m\theta + b^I_{m,n}\sin m\theta\right)\frac{J_m(\lambda_{m,n}r)\exp(iK_{m,n}z)}{N_{m,n}} \tag{13}$$

$$p^R(r,\theta,z) = \sum_{m=0}^{M}\sum_{n=0}^{N}\left(a^R_{m,n}\cos m\theta + b^R_{m,n}\sin m\theta\right)\frac{J_m(\lambda_{m,n}r)\exp(-iK_{m,n}z)}{N_{m,n}} \tag{14}$$

$$p^t(r,\theta,z) = \sum_{m=0}^{M}\sum_{n=0}^{N}\left(a^t_{m,n}\cos m\theta + b^t_{m,n}\sin m\theta\right)\frac{J_m(\lambda_{m,n}r)\exp[iK_{m,n}(z - L)]}{N_{m,n}} \tag{15}$$

and

$$K^2_{m,n} = K^2 - \lambda^2_{m,n} \tag{16}$$

whereas the solution for the circumferentially segmented liner is expressed in terms of the circumferential liner duct modes

$$P(r,\theta,z) = \sum_{\ell=0}^{\infty}\left\{A_\ell\exp(iK_\ell z) + B_\ell\exp\left[-iK_\ell(z - L)\right]\right\}P_\ell(r,\theta) \tag{17}$$

in which the eigenmode P_ℓ and the axial propagation constant K_ℓ are solutions to equations (9) to (11). The coefficients in the expansion for the incident wave are assumed to be known whereas those in the expansion for the waves in equations (14) to (17) have to be determined. It is instructive to note that B_ℓ would also be zero if the circumferentially lined section was infinitely long. (See eq. (5).) However, the finite termination of the lined section leads to reflections of the acoustic waves at $z = L$ as indicated by the additional term $B_\ell\exp\left[-iK_\ell(z - L)\right]$

in equation (17). Further, the length L has been included in equations (15) and (17) to assure that the waves running to the left and to the right attenuate properly in their direction of travel.

Physical considerations require that the acoustic pressure and the corresponding axial derivative remain continuous at each junction between the circumferential liner and the hard-wall duct. Such requirements ensure continuity to the first order of mass and momentum between adjacent duct segments. Expressed here in vector form,

$$\{E\} = \{0\}$$

where $\{0\}$ is a 4×1 null vector and $\{E\}$ is a 4×1 residual vector, as shown in the following:

$$\{0\} = \begin{Bmatrix} 0 \\ 0 \\ 0 \\ 0 \end{Bmatrix}$$

and

$$\{E\} = \begin{Bmatrix} E_1 \\ E_2 \\ E_3 \\ E_4 \end{Bmatrix}$$

where

$$E_1 = P^I(r,\theta,0) + P^R(r,\theta,0) - P(r,\theta,0)$$

$$E_2 = \frac{\partial P^I}{\partial z}(r,\theta,0) + \frac{\partial P^R}{\partial z}(r,\theta,0) - \frac{\partial P}{\partial z}(r,\theta,0)$$

$$E_3 = P(r,\theta,L) - P^t(r,\theta,L)$$

and

$$E_4 = \frac{\partial P}{\partial z}(r,\theta,L) - \frac{\partial P^t}{\partial z}(r,\theta,L)$$

The mode matching equations are obtained by requiring that the residual vector be orthogonal to each of the functions $P_\ell(r,\theta)$, or

$$\int_0^{2\pi}\int_0^1 \{E(r,\theta)\}\, P_\ell(r,\theta)\, r\, dr\, d\theta = \{0\} \qquad (\ell = 0, 1, 2, \ldots, N) \tag{18}$$

where

$$N = (2M + 1)(N + 1) - 1$$

Equation (18) constitutes a system of linear equations which can be expressed in matrix form as

$$[G]\{\phi\} = \{F\} \tag{19}$$

where $\{\phi\}$ contains the unknown coefficients of equations (14), (15), and (17) and $\{F\}$ contains the known coefficients in the expansion for the incident wave. (See eq. (13).) Furthermore, the order of this system of equations is $4(2M + 1)(N + 1)$. Equation (19) has been solved using Gaussian elimination to obtain $\{\phi\}$.

The transmission-loss function TL is still given by equations (7) and (8) for the finite circumferentially segmented liner as

$$TL = 10 \log_{10}[W(0)/W(L)]$$

However, the power of the incident wave is

$$W(0) = \sum_{m=0}^{M}\sum_{n=0}^{N}\left(\left|a^I_{m,n}\right|^2 + \left|b^I_{m,n}\right|^2\right)\mathrm{Re}(K_{m,n}) \tag{20}$$

Equation (20) is a general expression which assumes that the incident acoustic wave is composed of multiple circumferential modes. Transmission-loss values presented in the "Results and Discussion" section of this paper are for incident waves consisting

of only a single circumferential mode, $m = m_0$, so that the power of the incident wave reduces to

$$W(0) = W_{m_0}(0) \tag{21}$$

and

$$W_{m_0}(0) = \sum_{n=0}^{N} \left(\left| a^I_{m_0,n} \right|^2 + \left| b^I_{m_0,n} \right|^2 \right) \mathrm{Re}\left(K_{m_0,n} \right) \tag{22}$$

In addition, the output acoustic power is calculated from the transmitted acoustic wave for $z = L$ as

$$W(L) = \sum_{m=0}^{M} W_m(L) \tag{23}$$

and

$$W_m(L) = \sum_{n=0}^{N} \left(\left| a^t_{m,n} \right|^2 + \left| b^t_{m,n} \right|^2 \right) \mathrm{Re}(K_{m,n}) \tag{24}$$

Now cutoff modes have the property $\mathrm{Re}(K_{m,n}) = 0$ (i.e., $K \leq \lambda_{m,n}$) whereas cut-on modes have the property $\mathrm{Re}(K_{m,n}) > 0$. Thus, no acoustic energy is transported by cutoff modes. Hence, the summation in equations (20) to (24) actually reduces to summation for a finite number of cut-on modes. The transmission-loss function for a single circumferential-mode input becomes

$$TL = 10 \log_{10} \left[W_{m_0}(0) \Big/ \sum_{m=0}^{M} W_m(L) \right] \tag{25}$$

whereas the transmission-loss function for circumferential mode m is

$$TL_m = 10 \log_{10} \left[W_{m_0}(0) / W_m(L) \right] \tag{26}$$

Thus, TL_m represents the amount of incident acoustic energy that is scattered and then absorbed from circumferential mode m_0 to circumferential mode m. It should be noted that no scattering between modes of different circumferential-mode orders occurs for a uniform or axially segmented liner.

Optimization Method

An optimization method was used to design and study circumferentially segmented liners for specified modal inputs and source frequencies. Although a variety of optimization methods exists, good success has been obtained with the so-called Quasi-Newton optimization algorithms. These algorithms combine the best features of steepest ascent and Newton's method. Apparently, the Davidon-Fletcher-Powell (DFP) optimization algorithm has been the most commonly used in duct acoustics (refs. 2 and 3). Thus, the DFP optimization algorithm with the transmission-loss function $TL(\beta_1, \beta_2)$ as the optimization parameter is used here. The free variables in the algorithm were taken to be the resistance R and the reactance χ of the two admittance segments

$$\beta_1 = \frac{1}{R_1 + i\chi_1}$$

and

$$\beta_2 = \frac{1}{R_2 + i\chi_2}$$

However, contour maps were first obtained to provide good starting values for the algorithm. More detailed information on the optimization algorithm used herein is given in appendix B.

RESULTS AND DISCUSSION

Trend studies for both uniform and circumferentially segmented liners are presented. First, optimized segmented liners are presented and compared to optimized uniform liners for the semi-infinite duct depicted in figure 2. In order to reduce computational cost, optimization studies were performed only with $L = 2$. Second, studies are presented in which neither the uniform nor the segmented liner is optimized (i.e., off-optimum studies) with $L = 2$. These off-optimum trend studies include the effects of the two hard-wall sections (see fig. 4), so equations (23) and (24) are used to determine transmission losses. Finally, a cursory investigation of the effects of the lining length L is presented. These effects are investigated for the treated section installed within a hard-wall duct only. (See eqs. (23) and (24).)

Optimization Studies

Optimization results for the semi-infinite duct are presented in the following subsections. First, results for a plane wave input into a uniform liner are compared to results in an existing work to obtain confidence in the optimization method. Second, optimized segmented liners are compared with optimized uniform liners for a range of frequencies and source inputs. Segmented-liner studies consist of both hard-wall/soft-wall and soft-wall/soft-wall lining configurations.

Plane wave incident into uniform liner.- Optimum transmission-loss values for a plane wave source are compared to those computed from the exact analysis of reference 2 in figure 6. Excellent agreement between the two analyses is observed. Optimum liner properties computed from the two analyses are presented in figures 7 and 8. Although the optimum resistance values compare favorably, agreement for the optimum reactance deteriorates with increasing frequency. This analysis shows excellent agreement at low frequencies but yields higher values than reference 2 as the frequency increases. However, the differences in reactance fail to change the optimum transmission losses. Thus, there may be more than one value of admittance in the complex admittance plane which gives the same transmission-loss value.

Hard-wall/soft-wall optimization studies.- Figure 9 shows the optimum transmission-loss spectrum for a circumferentially segmented liner with different periodicities. The source is taken to be a plane wave with the optimum uniform liner used as a baseline for comparison. The width of the circumferential strips plays an important role in the liner performance. The performance of the segmented liner is an increasing function of the periodicity at each value of frequency. In addition, the uniform liner gives more suppression than the segmented liners. Note that the segmented-liner results approach the uniform-liner results as the periodicity increases. Optimum liner properties for the segmented liner are not presented. However, it was observed that β_{av} for the segmented liners with high periodicity simply approaches the optimum admittance for the uniform liner.

Optimum transmission losses are presented in figure 10 for a segmented and a uniform liner. The incident wave for both cases was chosen to have a circumferential mode of $m = 5$ $(Q(r,\theta) = \cos 5\theta\, J_5(\lambda_{5,0}r))$. The segmented liner has a periodicity of 5 so that the m numbers included in equation (12) are $m = 5, 10, 15, \ldots$ from the discussion in appendix A. As shown in figure 10, the uniform liner gives better performance than the segmented liner at the optimum point for all frequencies considered. Optimum liner properties for the liners are shown in figures 11 and 12. Figure 11 shows an interesting trend for the optimum conductance. (The conductance is the real part of the complex admittance.) Note that the optimum conductance of the uniform and segmented liners are approximately equal. On the other hand, figure 12 shows that the optimum susceptance of the two liners does not show such trends (i.e., the susceptance is the negative value of the imaginary part of the complex admittance).

We now turn to optimization studies at the higher frequencies for which high m-number sources are possible. A cursory investigation of the matrices of equation (A9) reveals that the off-diagonal terms of these matrices increase in magnitude with increasing frequency, so that stronger coupling between the m numbers might be expected at the higher frequencies than the lower ones. Figure 13 compares the transmission losses for a uniform and a segmented liner. The source for both liners was a circumferential mode of $m = 10$ $(Q(r,\theta) = \cos 10\theta\, J_{10}(\lambda_{10,0}r))$ with the periodicity of the segmented liner equal to 10 $(T = 10)$. The segmented liner gives greater broadband performance than the uniform liner. Further, the performance

of the segmented liner approaches that of the uniform liner as the frequency gets closer to the cut-on value of the m number of the source. The optimum conductance and the optimum susceptance for the uniform and segmented liners are depicted in figures 14 and 15. Optimum conductance values for both the uniform and the segmented liner decrease in magnitude with increasing frequency; however, the segmented-liner values are higher than the uniform-liner values. Optimum susceptance values for the uniform liner approach zero at most frequencies. In contrast, the optimum susceptance values for the segmented liner vary with frequency from 0.29 to 0.62.

Figure 16 shows a comparison of the optimum transmission-loss spectrums for a uniform and a segmented liner in which the circumferential mode order of the source is 15 ($Q(r,\theta) = \cos 15\theta\, J_{15}(\lambda_{15,0}r)$). Note that the segmented liner gives higher transmission losses than the uniform liner. Optimum conductance values for the uniform and the segmented liner are shown in figure 17. Results in this figure show that the conductance of the segmented liner is roughly twice that of the uniform liner. Optimum susceptance values for the two liners are given in figure 18 and show trends consistent with figure 13. Note that the optimum susceptance of the uniform liner is approximately zero, whereas that of the segmented liner is not.

Soft-wall/soft-wall optimization studies.- The results presented so far restricted one section of the segmented liner to be a hard wall so that β_2 was zero. Studies were also performed in which β_1 and β_2 were varied in the optimization algorithm. This lining configuration for which β_2 is not restricted to zero is referred to as the soft-wall/soft-wall circumferentially segmented liner. Further, results for the soft-wall/soft-wall segmented liner were computed for the same sources as for the hard-wall/soft-wall optimization studies. Optimum properties for the plane-wave source and the source with circumferential dependence of $m = 5$ converge with the uniform-liner optimum properties where $\beta_1 = \beta_2$. Although at some frequencies the admittances were different, the optimum transmission loss for the segmented liner was the same as the uniform liner to within 1 dB. A significant result was obtained for the sources with $m = 10$ and $m = 15$. For these sources, the optimization algorithm shows that $\beta_2 = 0 + 0i$ was the optimum β_2 with β_1 being identical to the value obtained from the hard-wall/soft-wall optimization studies. Further, for the frequencies in figure 13 for which the uniform liner gave slightly higher transmission losses than the segmented liner, the fully treated segmented-liner results converged with the uniform-liner values where $\beta_1 = \beta_2$. Thus, a uniform liner stripped with aluminum tape may provide the best method of increasing the performance of a uniform liner for high m-number sources. Further, removing the strips of aluminum tape and installing acoustic treatment may actually decrease the performance of the liner.

Off-Optimum Studies

In order to verify the accuracy of the mode matching equations used herein, sample calculations for a uniform liner with $L = 2$ were computed and compared to results obtained from the analysis of Zorumski (ref. 1). Computations obtained from Zorumski's analysis were based on the assumption that the superposition of 10 soft-wall modes could adequately represent the incident wave. In addition, the version of Zorumski's analysis used included only single interface effects. Therefore, for comparison purposes, mode matching equations were developed for a single interface so that the second hard-wall section (see fig. 5) was removed and replaced by a nonreflecting termination at $z = L$.

Values from sample calculations are presented in figure 19 for an incident plane wave ($P^I(r,\theta,0) = 1$). The admittance values used at each frequency to compute the transmission losses are optimum for no reflections at $z = L$. As depicted in figure 19, excellent agreement between this analysis and that of reference 1 is obtained. A plot of values from a second sample calculation is presented in figure 20. Although the admittance values used to obtain the transmission losses in figure 20 are the same as those used in figure 19, the incident wave has been changed to

$$P^I(r,\theta,0) = \cos\ \theta\ J_1(\lambda_{1,0}r)$$

Discrepancies of about 11 percent at $K = 4$ and 26 percent at $K = 5$ are observed in the transmission losses computed from this analysis and that of Zorumski. Excellent agreement is obtained for $K > 5$. Further, it should be noted that by increasing N from 9 to 20, the discrepancy at $K = 4$ was reduced to less than 2 percent, though no significant improvement in the discrepancy at $K = 5$ was observed. It is believed this discrepancy can be removed by a superposition of more than 10 soft-wall modes to represent the incident wave in Zorumski's analysis. Overall, good agreement has been obtained between this analysis and the analysis used in reference 1. This leads to a degree of confidence in the mode matching equations developed in this paper.

Having developed confidence in the analysis, we can now proceed to show that the analysis gives results consistent with the experimental observations of Mani (ref. 5). Figure 21 compares transmission-loss values for a uniform and a segmented liner but for an incident wave with $m = 10$ ($P^I(r,\theta,0) = \cos 10\theta\ J_{10}(\lambda_{10,0}r)$). Values were computed for $L = 2$ with equation (25) being used to compute the transmission-loss spectrum. The uniform-liner admittance was set equal to β_1, where the conductance and susceptance vary with frequency as shown in figures 13 and 14. The segmented-liner admittance function was obtained by setting $T = 10$, $\beta_2 = 0 + 0i$, and β_1 the same as the uniform liner (i.e., the segmented liner is simply the uniform liner stripped with 10 evenly spaced strips of aluminum tape). As depicted in figure 21, significant increases in performance can be realized by stripping the uniform liner, particularly at the frequencies closest to cut on of the $m = 10$ circumferential mode. It must be emphasized that the increased suppression of the segmented liner over the uniform liner as depicted in figure 21 may not hold generally since the admittance β_1 was deliberately chosen so that the segmented liner was optimized. Thus, different values of the admittance β_1 may show the uniform liner to be superior to the segmented one. This may, however, be representative of the effect observed by Mani in reference 5.

A more rigorous comparison of the performance of a uniform and a segmented liner is obtained when both liners are optimized, or tuned, at a fixed frequency. This allows a comparison of the off-optimum performance of the two liners. Figure 22 compares the transmission-loss spectrum for a uniform and a segmented liner with a hard-wall/soft-wall admittance variation. Both the uniform and the segmented liner are tuned at $K = 20$ so that they are optimum only at this frequency. The segmented liner gives better performance not only at the tuning frequency, $K = 20$, but at other frequencies as well. Similar trends were observed when the tuning frequency of the two liners was $K = 18$ and $K = 16$.

Effects of Duct Length

Figures 23, 24, and 25 compare the transmission-loss spectrums computed from equation (25) for a uniform and a segmented liner for $L = 1/2$, 1, and 2. The incident wave for the figures was chosen to be $P^I(r,\theta,0) = \cos 5\theta\, J_5(\lambda_{5,0}r)$ whereas the admittance function for the segmented liner was chosen so that $T = 5$, $\beta_2 = 0$, and $\beta_1 = 1.00 - 0.62i$ (i.e., β_1 is an arbitrarily chosen value). The admittance of the uniform liner was the same as β_1 for the segmented liner. Thus, the segmented-liner configuration can be obtained by stripping the uniform liner with tape. (This is the configuration proposed by Mani in ref. 5.) One can see from the figures that the segmented-liner performance increases relative to the uniform liner as dimensionless duct length increases. For $L = 2$, the segmented liner performs better than the uniform liner at all frequencies considered. This is surprising since only 50 percent of the segmented liner is treated (i.e., $\beta_2 = 0$).

The total and modal transmission losses (see eqs. (25) and (26)) are probably also strongly affected by the duct length L. Figure 26 illustrates total and modal transmission losses obtained for a segmented liner as a function of dimensionless duct length. The computer calculations were made with $K = 4.4$, $\beta_2 = 0 + 0i$, $\beta_1 = 1 + 2i$, $T = 1$, and $P^I(r,\theta,0) = \cos\theta\, J_1(\lambda_{1,0}r)$. Equations (25) and (26) were used to compute the transmission losses so that the effects of both hard-wall interfaces are included. Results in the figure show that the circumferentially segmented liner has scattered acoustic energy into higher order circumferential modes than those present at the source. Since TL_3 is at least 10 dB above TL_2 and TL_1, only a small portion of the total power is carried by the $m = 3$ mode in the second hard-wall section. Note also that TL_1 and TL_2 are approximately equal when $1 \leqslant L \leqslant 2$. Thus, the circumferentially segmented liner has distributed energy equally between the $m = 1$ and $m = 2$ modes in the second hard-wall section for this range of L values.

CONCLUSIONS

Optimum and off-optimum properties of circumferentially segmented duct liners have been compared with those of uniform liners to analyze possible benefits of circumferential segmentation. Based on the results of this work, the following conclusions have been made:

1. Circumferentially segmented liners scatter acoustic energy among various circumferential wave numbers m. Results indicate that for some frequencies and duct lengths, the segmented liner may scatter source energy equally between a lower and higher order circumferential wave number.

2. For low m-number sources, there is no advantage to an optimized circumferentially segmented liner over an optimized uniform liner.

3. For high m-number sources, an optimized circumferentially segmented liner gives better performance than an optimized uniform liner.

4. Segmented-liner configurations consisting of a hard-wall/soft-wall combination represent an optimum configuration for high m-number sources. Thus, replacing the hard-wall strips with acoustic treatment may decrease the performance of the liner.

5. Overall, the greatest benefit of circumferentially segmented liners over uniform liners occurred away from the optimum point. Off the optimum point, segmented liners give more effective broadband performance with a 50-percent reduction in the amount of acoustic treatment.

6. Increases in performance of the segmented liner relative to the uniform liner are greatest at frequencies closest to cut on of the circumferential mode number of the source.

It should be emphasized that optimization studies were for a duct length-to-radius ratio of 2, so these conclusions may not hold for all duct lengths. Results presented here are sufficiently encouraging (particularly for the high m-number sources) to warrant further studies involving circumferentially segmented liners in series or in checkerboard liners, the effects of multiple m-number sources, and the convective and refractive effect of a mean flow.

Langley Research Center
National Aeronautics and Space Administration
Hampton, VA 23665
August 2, 1982

APPENDIX A

EXACT SOLUTION FOR CIRCUMFERENTIALLY SEGMENTED LINER

This appendix presents the derivation of the exact solution to the elliptic partial differential equation (eq. (9))

$$\nabla^2 P_\ell(r,\theta) + \lambda_\ell^2 P_\ell(r,\theta) = 0$$

and boundary condition

$$R_b(\theta) = 0 \tag{A1}$$

where

$$R_b(\theta) = \frac{\partial P_\ell(1,\theta)}{\partial r} - iK\,\beta(\theta)\,P_\ell(1,\theta) \tag{A2}$$

and

$$\beta(\theta) = \frac{\beta_1 + \beta_2}{2} + \frac{2(\beta_1 - \beta_2)}{\pi}\left(\sin T\theta + \frac{\sin 3T\theta}{3} + \frac{\sin 5T\theta}{5} + \ldots\right) \tag{A3}$$

The goal of the derivation of this equation is to show how the periodicity of the acoustic liner T selects preferred values of circumferential mode orders. This is of great utility in that it provides greater physical insight into how source energy is redistributed into higher circumferential mode orders and it may lead to more realistic design criteria.

It is easily verifiable that each of the functions $\cos m\theta\, J_m(\lambda_\ell r)$ and $\sin m\theta\, J_m(\lambda_\ell r)$ is a solution to equation (9). Thus, the most general solution to this equation is obtained by using the superposition principle

$$P_\ell(r,\theta) = \sum_{m=0}^{\infty}\left(A_m^\ell \cos m\theta + B_m^\ell \sin m\theta\right) J_m(\lambda_\ell r) \tag{A4}$$

Although arbitrary values of the parameters A_m^ℓ, B_m^ℓ, and λ_ℓ satisfy equation (9), only selected values of these parameters will satisfy the boundary conditions imposed by the circumferentially segmented liner (eq. (A1)). Thus, it is still a matter of considerable mathematical difficulty to find the discrete values of the coefficients A_m^ℓ and B_m^ℓ and of eigenvalue λ_ℓ which cause the boundary residual $R_b(\theta)$ to vanish as indicated by equation (A1).

APPENDIX A

To satisfy the boundary condition imposed by the circumferentially segmented liner, one can make use of the fact that the set of functions (cos $m\theta$, sin $m\theta$) represents a complete set on the interval 0 to 2π and that only the zero function can be orthogonal to each member of a complete set. It is necessary that

$$\int_0^{2\pi} R_b(\theta) \cos m\theta \, d\theta = 0 \qquad (m = 0, 1, \ldots) \tag{A5}$$

and

$$\int_0^{2\pi} R_b(\theta) \sin m\theta \, d\theta = 0 \qquad (m = 1, 2, \ldots) \tag{A6}$$

Equations (A5) and (A6) are an alternate way of satisfying equation (A1) and are based on Galerkin's method (ref. 10). Further, the collection of equations (A5) and (A6) for each circumferential mode order m forms a set of simultaneous equations that can be expressed as

$$[D]\{X\} = \{0\} \tag{A7}$$

where $[D]$ is the complex coefficient matrix, $\{X\}$ is the unknown vector of Fourier coefficients, and $\{0\}$ is the null vector. Ordinarily, equation (A7) is solved to obtain the unknown vector $\{X\}$ and the eigenvalue λ_ℓ is determined by requiring that the determinant of the coefficient matrix vanish. It will now be shown that only a subset of this more general equation need be solved for any given source.

The detailed structure of the matrix equation given by equation (A7) for a liner with periodicity T is

$$[D] = \begin{bmatrix} [D_0] & & & & \\ & \ddots & & & \\ & & [D_1] & & \\ & & & \ddots & \\ & & & & [D_T] \end{bmatrix}$$

$$\{X\}^T = \left[X_0^T, X_1^T, X_2^T, \ldots, X_T^T\right]$$

where $[D_s]$ is a square matrix, $\{X_s\}$ is an unknown vector of the same order as $[D_s]$, subscript s is the index $0, 1, \ldots, T$, and the superscript T denotes the

transpose. The diagonal character of [D] implies the periodicity of the acoustic liner decouples equation (A7) into (T + 1) eigenvalue problems

$$\left.\begin{aligned} [D_0]\{X_0\} &= \{0\} \\ [D_1]\{X_1\} &= \{0\} \\ [D_2]\{X_2\} &= \{0\} \\ &\vdots \\ [D_T]\{X_T\} &= \{0\} \end{aligned}\right\} \tag{A8}$$

where the vectors $\{X_s\}$ are

$$\{X_s\}^T = \begin{cases} [A_s^\ell, A_{2T-s}^\ell, A_{4T-s}^\ell, \ldots, B_{T-s}^\ell, B_{T+s}^\ell, B_{3T-s}^\ell, \ldots] & (s = 1, 2, \ldots, T-1) \\ [A_0^\ell, A_{2T}^\ell, A_{4T}^\ell, \ldots, B_T^\ell, B_{3T}^\ell, B_{5T}^\ell, \ldots] & (s = 0) \\ [A_T^\ell, A_{3T}^\ell, A_{5T}^\ell, \ldots, B_{2T}^\ell, B_{4T}^\ell, B_{6T}^\ell, \ldots] & (s = T) \end{cases}$$

where superscript ℓ indicates the exact eigenfunction index. Thus, each subeigenvalue problem $[D_s]\{X_s\} = \{0\}$ can be solved independently of each other and the eigenfunctions $P_\ell(r,\theta)$ for each subproblem are mutually orthogonal. This means that the only subproblems which need to be solved for any given source are those which contain the circumferential mode orders of the source. For example, only the subeigenvalue problem $[D_0]\{X_0\} = \{0\}$ needs to be solved for an axisymmetric (circumferentially uniform) source. Further, the matrices $[D_s]$ should be truncated at some finite order. (For example, results in the text use only the first six circumferential mode orders so that $[D_s]$ will be of order six.) Eigenvalues for each subproblem are obtained by setting each determinate in equation (A8) to zero

$$\det[D_s] = 0 \qquad (s = 0, 1, \ldots, T)$$

so that these determinants determined the exact transcendental equations for a circumferentially segmented liner. Note also that the exact transcendental equation for a uniform liner is obtained by setting $\beta_1 = \beta_2$ and allowing the periodicity to approach infinity. Under these conditions

$$\det[D_s] = J_s'(\lambda_\ell) - iK\beta_1 J_s(\lambda_\ell) \qquad (s = 0, 1, \ldots)$$

so that results here do degenerate to the exact solution for uniform liners.

APPENDIX B

DAVIDON-FLETCHER-POWELL (DFP) OPTIMIZATION ALGORITHM

In this appendix, more detailed information concerning the optimization of the transmission-loss function is presented. This transmission-loss function is expressed in terms of an admittance vector $TL(\beta_1,\beta_2) = TL\{d\}$, where $\{d\}$ is the 4×1 admittance vector

$$\{d\} = \begin{Bmatrix} R_1 \\ \chi_1 \\ R_2 \\ \chi_2 \end{Bmatrix}$$

Starting with an initial admittance vector $\{d^k\}$, in which the superscript k is an iteration counter, it is the purpose of the DFP algorithm to move in a direction specified by the ascent vector $\{\delta^k\}$ so that a greater value of the transmission loss is obtained at the next value of the admittance vector $\{d^{k+1}\}$. The steps in the DFP algorithm (ref. 11) are as follows:

1. Start with an initial admittance vector $\{d^0\}$ and any 4×4 symmetric positive-definite matrix $[H^0]$. (Here, $[H^0]$ was chosen as the identity matrix.)

2. Beginning with $k = 0$, compute $\{\delta^k\} = -[H^k]\{g^k\}$, where $\{g^k\}$ is the gradient vector of TL at $\{d^k\}$.

3. Obtain the parameter α^k which maximizes

$$TL(\{d^k\} + \alpha^k\{\delta^k\})$$

4. Set

$$\{d^{k+1}\} = \{d^k\} + \alpha^k\{\delta^k\}$$

$$\{y^k\} = \{g^{k+1}\} - \{g^k\}$$

and

$$[H^{k+1}] = [H^k] + \frac{\alpha^k\{\delta^k\}\{\delta^k\}^T}{\{\delta^k\}\{y^k\}} - \frac{[H^k]\{y^k\}\{[H^k]\{y^k\}^T\}}{\{y^k\}[H^k]\{y^k\}}$$

where the superscript T denotes transpose.

5. Set $k = k + 1$ and return to step 1.

APPENDIX B

For this work, the iteration process was continued until the difference between $\{d^{k+1}\}$ and $\{d^k\}$ was at least 10^{-2}. Note that the square matrix $[H^k]$ is updated at each iteration in an attempt to have the algorithm converge more rapidly than the method of steepest ascent (in which case $[H^k]$ is the identity matrix) and in an attempt to be computationally more efficient than Newton's method (in which case $[H^k]$ is the inverse of the matrix of second partials, or the inverse Hessian matrix, for which evaluation is either too costly or impractical).

Although the DFP algorithm has worked well in the past on duct transmission problems, there are still defects in the method which should be considered when optimizing acoustic liners. For example, steps 2 and 4 require the computation of the gradient of the transmission-loss function, $TL(\{d^k\})$. This gradient must be computed numerically and the error in the numerical computation affects the convergence of the algorithm. In this paper the gradient was computed by finite differencing. On the other hand, step 3 of the DFP algorithm requires that the function $TL(\{d^k\} + \alpha^k\{\delta^k\})$ be maximized to determine the search parameter α^k. However, since this function cannot be maximized analytically, numerical techniques must be used, which in turn leads to inaccuracies in the search parameter α^k. Such inaccuracies in α^k can cause the algorithm to diverge or wander about meaninglessly in the admittance plane. The method of repeated parabolic interpolation was used in this paper to determine α^k in step 3 of the DFP algorithm. Generally, it has been the author's experience that no major problems with the algorithm occur with the method of computing the parameter α^k and transmission-loss gradient $\{g^k\}$ used here. A major problem did occur with the initialization vector $\{d^0\}$ because the DFP algorithm is not globally convergent. Originally, the optimum uniform values were used to initialize the algorithm; however, these values proved to be a local optimum, and larger transmission-loss values could be obtained by initializing the algorithm at nonuniform values.

To alleviate the problems associated with the initialization of the DFP algorithm, an alternate method (henceforth referred to as the DFPC method) has been used. In the DFPC method, a locus of two-dimensional contours is used to obtain initialization values which are close to global optimums. These initialization values are then used as inputs to the DFP optimization algorithm. The steps in the DFPC method are the following:

1. Vary R_2 and χ_2 from 1 to 10 in increments of 0.1.

2. Obtain the optimum β_1 and transmission-loss value at each increment on R_2 or χ_2 by contour mapping.

3. Obtain the global optimum from the loci of optimums obtained at each value of β_2.

4. Now use the DFP algorithm with the global optimums obtained from step 3 as starting values.

Although the DFPC method gives global optimum values, it will be quite expensive because a contour map must be obtained at each value of β_2. Generally, results presented herein use 10 points on both the real and the imaginary axis of β_1 to obtain the contour maps in which the increment spacing in both directions was unity. However, at some frequencies the increment spacing had to be reduced further to obtain smooth contours, particularly at frequencies near cut on.

REFERENCES

1. Zorumski, William E.: Acoustic Theory of Axisymmetric Multisectioned Ducts. NASA TR R-419, 1974.

2. Lester, Harold C.; and Posey, Joe W.: Optimal One-Section and Two-Section Circular Sound-Absorbing Duct Liners for Plane-Wave and Monopole Sources Without Flow. NASA TN D-08348, 1976.

3. Sawdy, David T.; Beckemeyer, Roy J.; and Patterson, John D.: Optimum Segmented Acoustic Liners for Flow Ducts. Paper D6, 90th Meeting Acoust. Soc. America (San Francisco, Calif.), Nov. 1975.

4. Baumeister, Kenneth J.: Optimized Multisectioned Acoustic Liners. NASA TM-79028, 1979.

5. Mani, Ramani: Acoustic Duct With Peripherally Segmented Acoustic Treatment. U.S. Pat. 3,937,590, Feb. 10, 1976.

6. Watson, Willie R.: A Finite Element Simulation of Sound Attenuation in a Finite Duct With A Peripherally Variable Liner. NASA TM-74080, 1977.

7. Astley, R. J.; Walkington, N. J.; and Eversman, W.: Transmission in Flow Ducts With Peripherally Varying Linings. AIAA-80-1015, June 1980.

8. Namba, M.; and Fukushige, K.: Application of the Equivalent Surface Source Method to the Acoustics of Duct Systems With Non-Uniform Wall Impedance. J. Sound & Vib., vol. 73, no. 1, Nov. 8, 1980, pp. 125-146.

9. Watson, Willie R.: Noise Suppression Characteristics of Peripherally Segmented Duct Liners. NASA TP-1904, 1981.

10. Finlayson, Bruce, A.: The Method of Weighted Residuals and Variational Principles With Application in Fluid Mechanics, Heat and Mass Transfer. Academic Press, Inc., c.1972.

11. Luenberger, David G.: Introduction to Linear and Nonlinear Programming. Addison-Wesley Pub. Co., Inc., c.1973.

SYMBOLS

A_ℓ, B_ℓ	amplitude of right and left moving wave in circumferentially segmented liner
A_m^ℓ, B_m^ℓ	coefficients in exact expansion of eigenfunction $P_\ell(r,\theta)$
$A_{m,n}^\ell, B_{m,n}^\ell$	coefficients in hard-wall duct expansion of the exact eigenfunction $P_\ell(r,\theta)$
a	duct radius
$a_{m,n}^I, b_{m,n}^I$	coefficients of Bessel-Fourier expansion of incident wave in first hard-wall section
$a_{m,n}^R, b_{m,n}^R$	coefficients of Bessel-Fourier expansion of reflected wave in first hard-wall section
$a_{m,n}^t, b_{m,n}^t$	coefficients of Bessel-Fourier expansion of transmitted wave in second hard-wall section
c	ambient speed of sound
d_n	coefficient in hard-wall duct expansion of Bessel function $J_m(\lambda_\ell)$
$\{d\}$	complex admittance vector
$\{d^k\}$	complex admittance vector with iteration k
$[D], [D_s], [G]$	complex coefficient matrices
$\{E\}$	residual vector
E_1, E_2, E_3, E_4	components of residual vector $\{E\}$
$\{F\}$	known-constant vector
$\{g^k\}$	gradient of transmission-loss function with iteration k
$[H^k]$	symmetric positive-definite matrix of order k
i	unit imaginary number
J_m	Bessel function of first kind of order m
K	wave number
$K_\ell, K_{m,n}$	axial wave numbers
L	predetermined length over which transmission loss is computed

M,N	total numer of m and n values
m	$= 0, 1, \ldots, M - 1$
$N_{m,n}$	normalization constant for hard-wall basis functions
n	$= 0, 1, \ldots, N - 1$
$P(r,\theta,z)$	acoustic pressure field in duct with circumferentially segmented liner
$P^I(r,\theta,z), P^R(r,\theta,z)$	incident and reflected pressure field in first hard-wall section
$P_\ell(r,\theta)$	acoustic pressure eigenfunction
$P^t(r,\theta,z)$	transmitted wave in second hard-wall section
$Q(r,\theta)$	source pressure function in semi-infinite duct
R	resistance of segmented liner
$R_b(\theta)$	boundary residual
$Re(\ )$	real part of complex expression
r,z	radial and axial coordinates
T	periodicity of segmented liner
$TL(\beta_1,\beta_2)$	total transmission-loss function
TL_m	transmission loss of circumferential mode m
t	time
$W(z)$	total sound power at axial location z
$W_m(z)$	sound power in circumferential mode m at axial location z
$\{X\}, \{X_s\}$	unknown-constant vectors
α^k	search parameter
$\beta(\theta), \beta_1, \beta_2$	acoustic admittances
β_{av}	average admittance for circumferentially segmented liner
$\{\delta^k\}$	ascent vector with iteration k
$\lambda_\ell, \lambda_{m,n}$	eigenvalues of circumferentially segmented and hard-wall duct
ρ	ambient density
$\{\phi\}$	unknown vector

ω	angular frequency
χ	reactance of segmented liner
∇^2	Laplace operator

Subscripts:

ℓ	exact eigenfunction index
m	circumferential wave number index
n	radial eigenfunction index for hard-wall duct
s	subeigenvalue problem index, $s = 0, 1, \ldots, T$

Superscripts:

k	iteration index
T	transpose operator

A bar over a symbol denotes a dimensional quantity. A prime denotes derivative with respect to the argument.

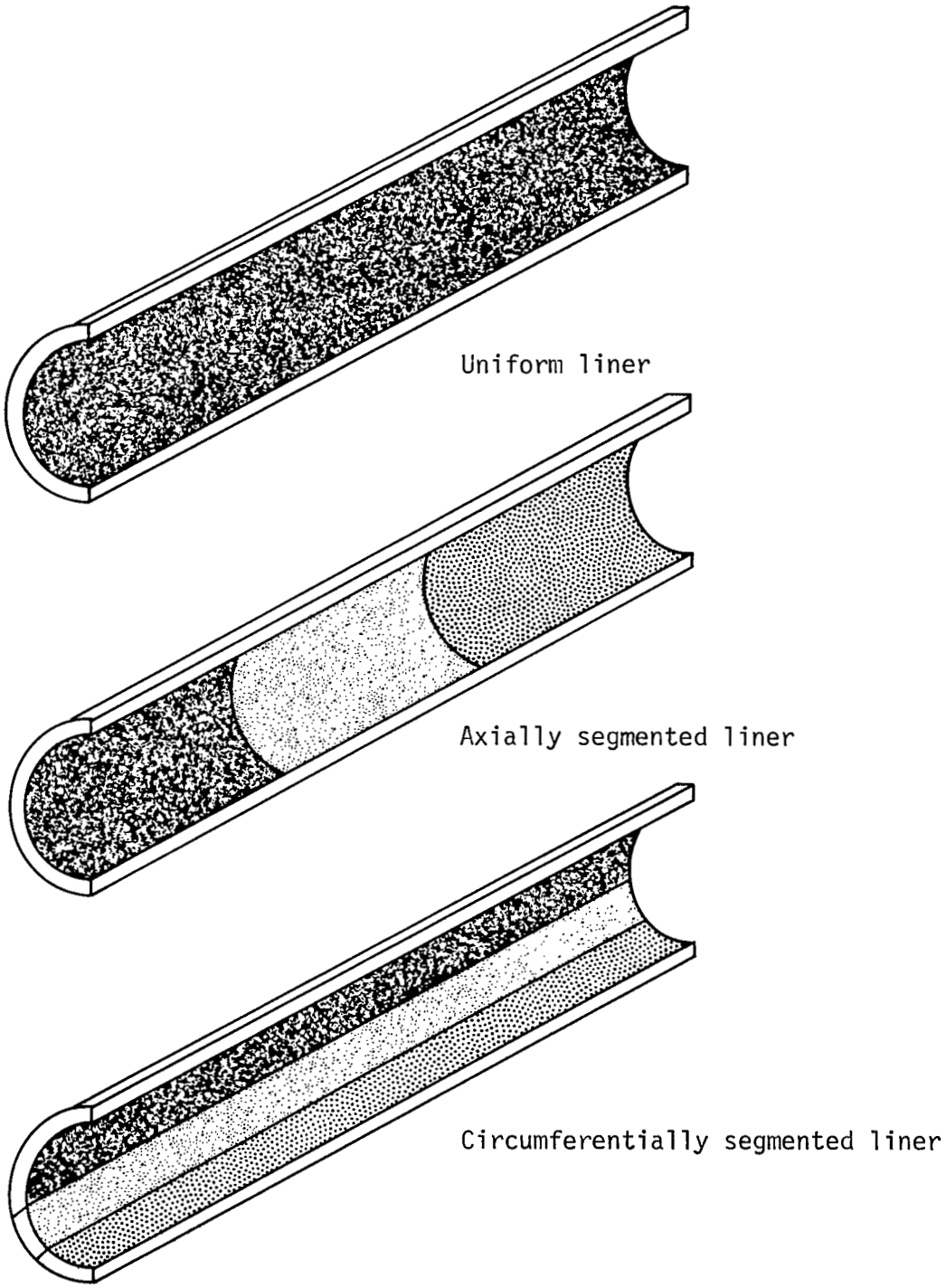

Figure 1.- Duct liner concepts.

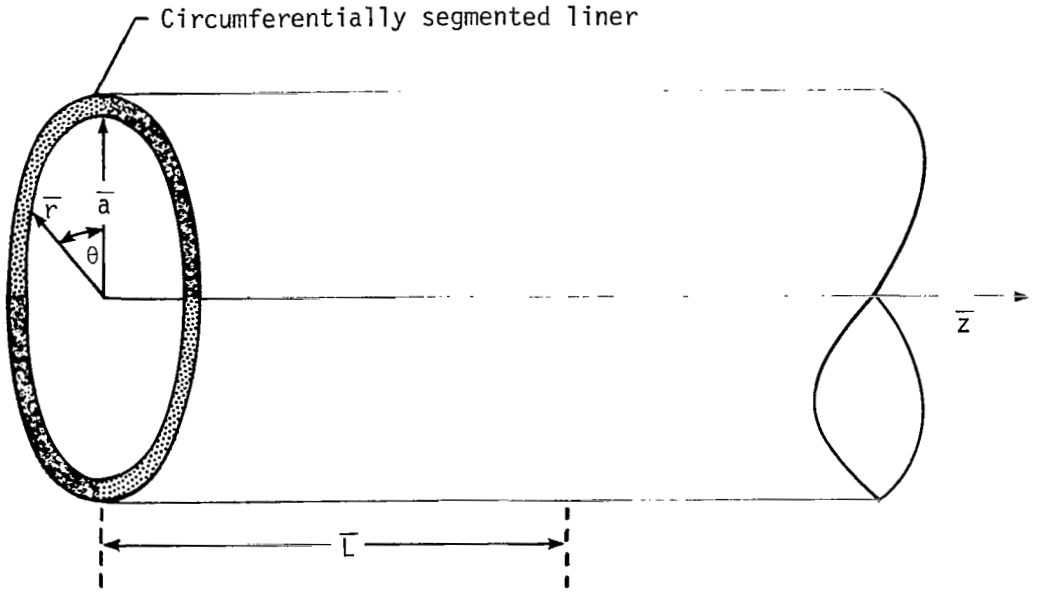

Figure 2.- Semi-infinite circular duct with circumferentially segmented liner and coordinate system.

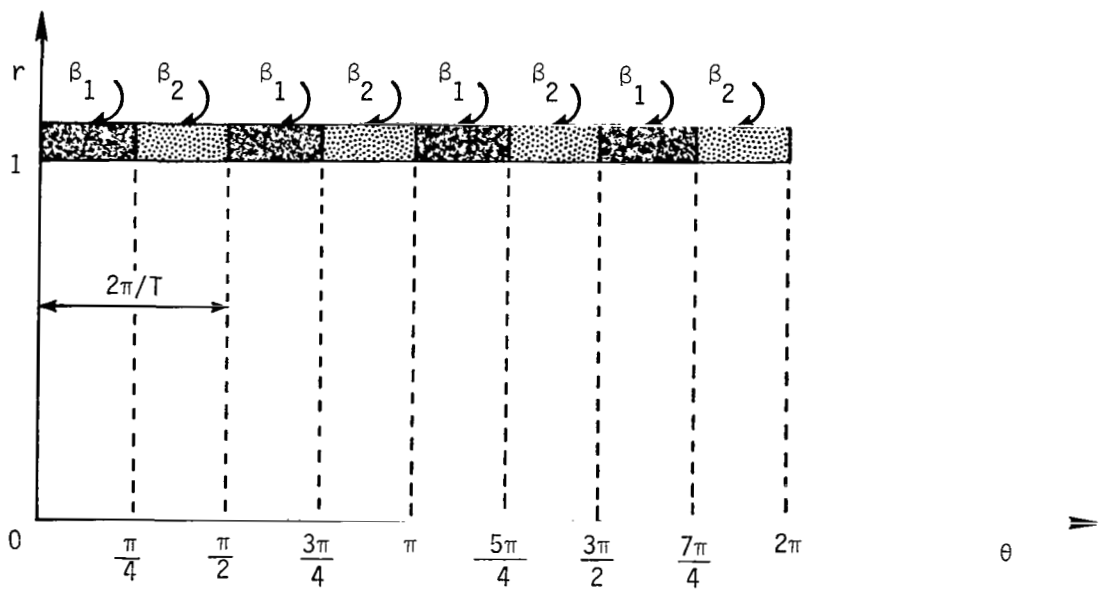

Figure 3.- Circumferentially segmented liner with periodicity T = 4.

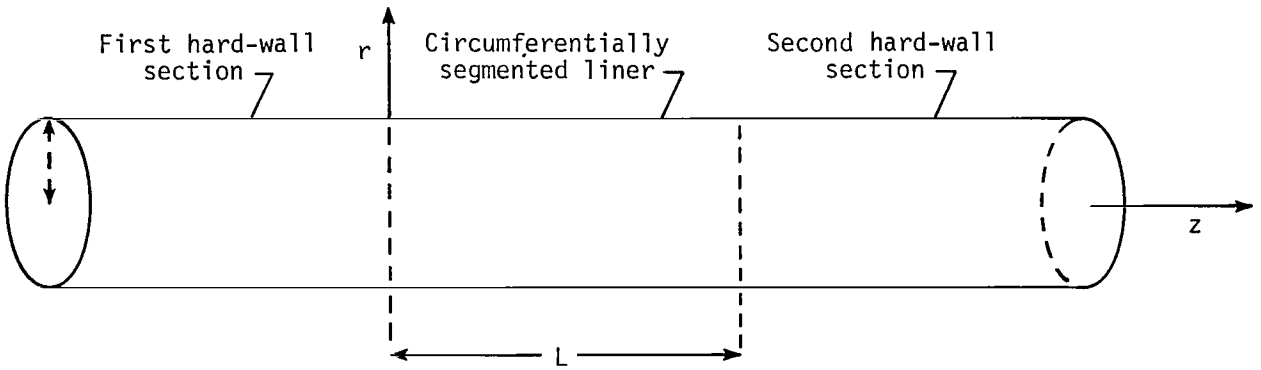

Figure 4.- Circumferentially segmented liner installed in hard-wall duct.

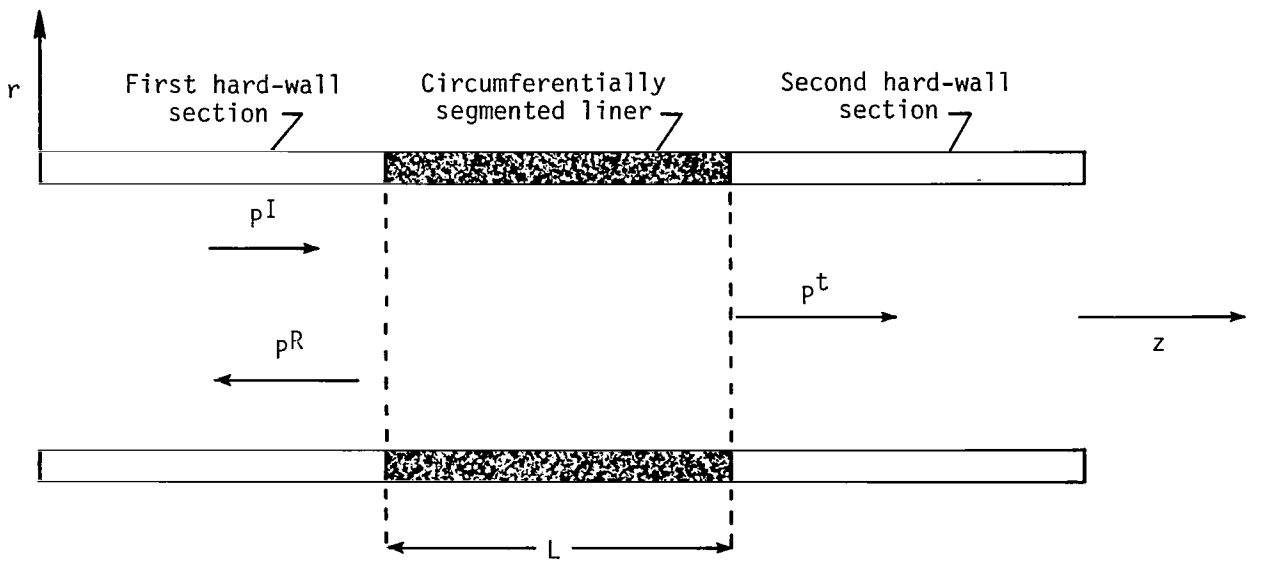

Figure 5.- Configuration used to develop mode matching equations.

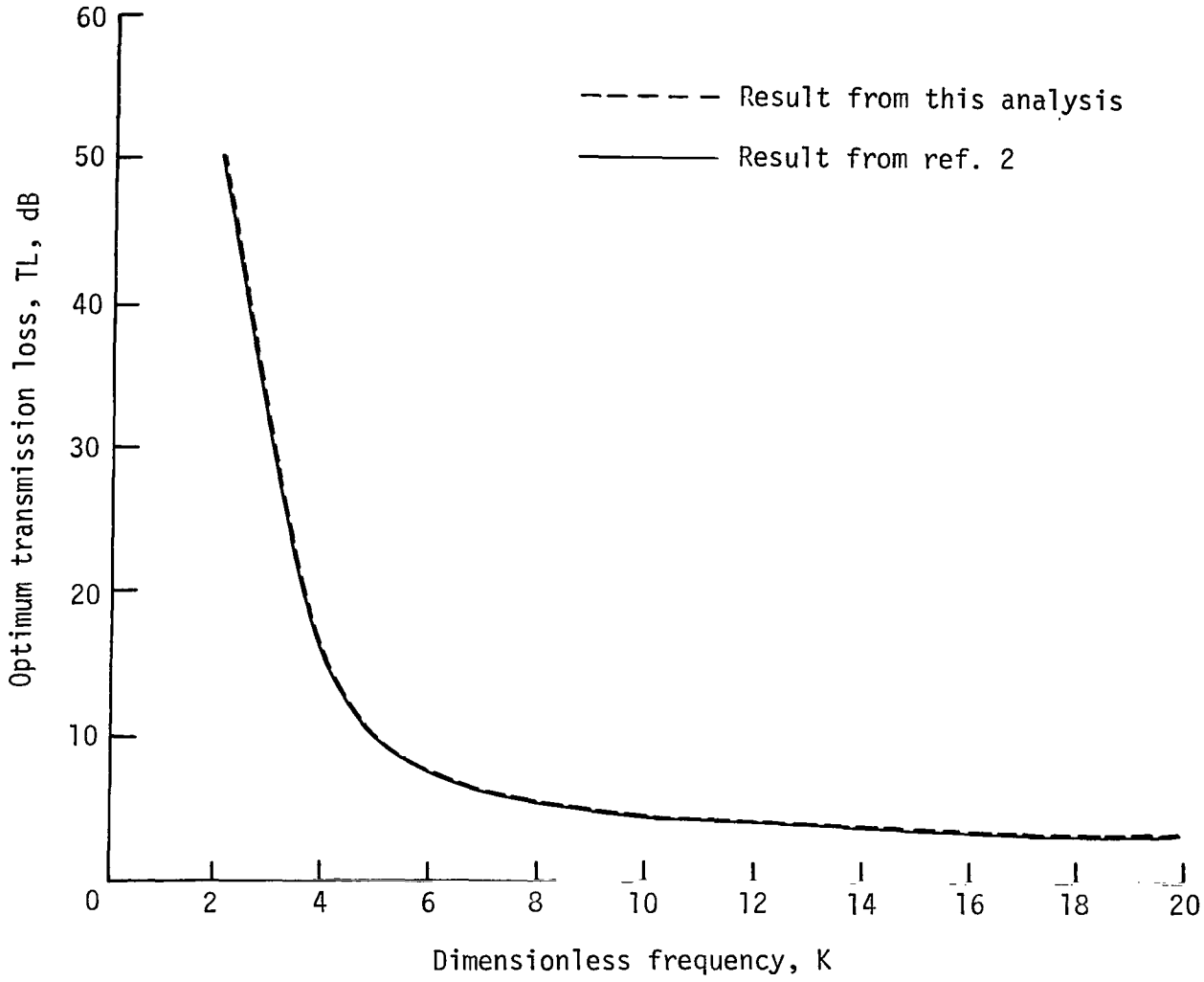

Figure 6.- Optimum transmission-loss spectrum for plane wave incident into an infinite uniform liner.

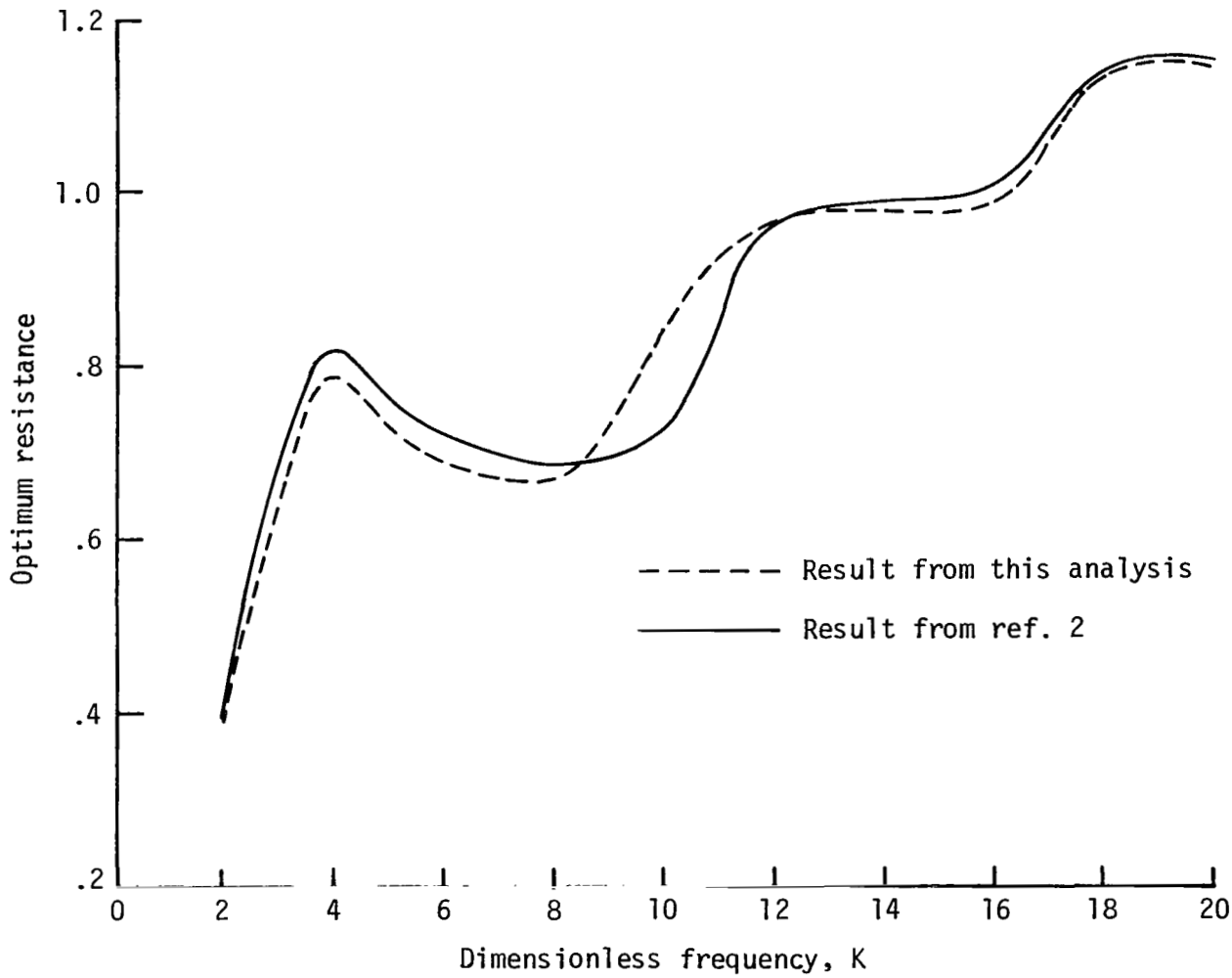

Figure 7.- Optimum resistance for transmission-loss spectrum of figure 6.

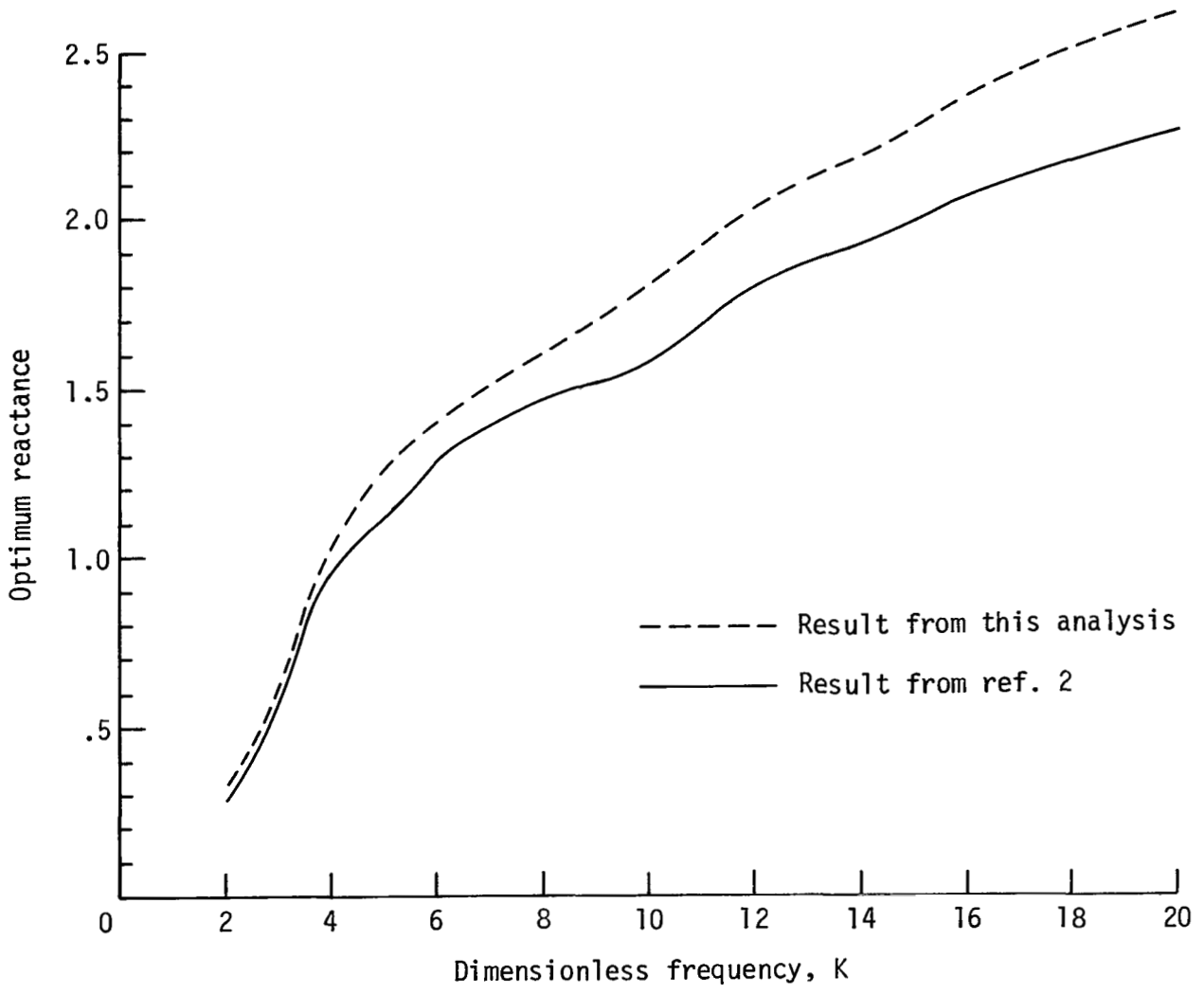

Figure 8.- Optimum reactance for transmission-loss spectrum of figure 6.

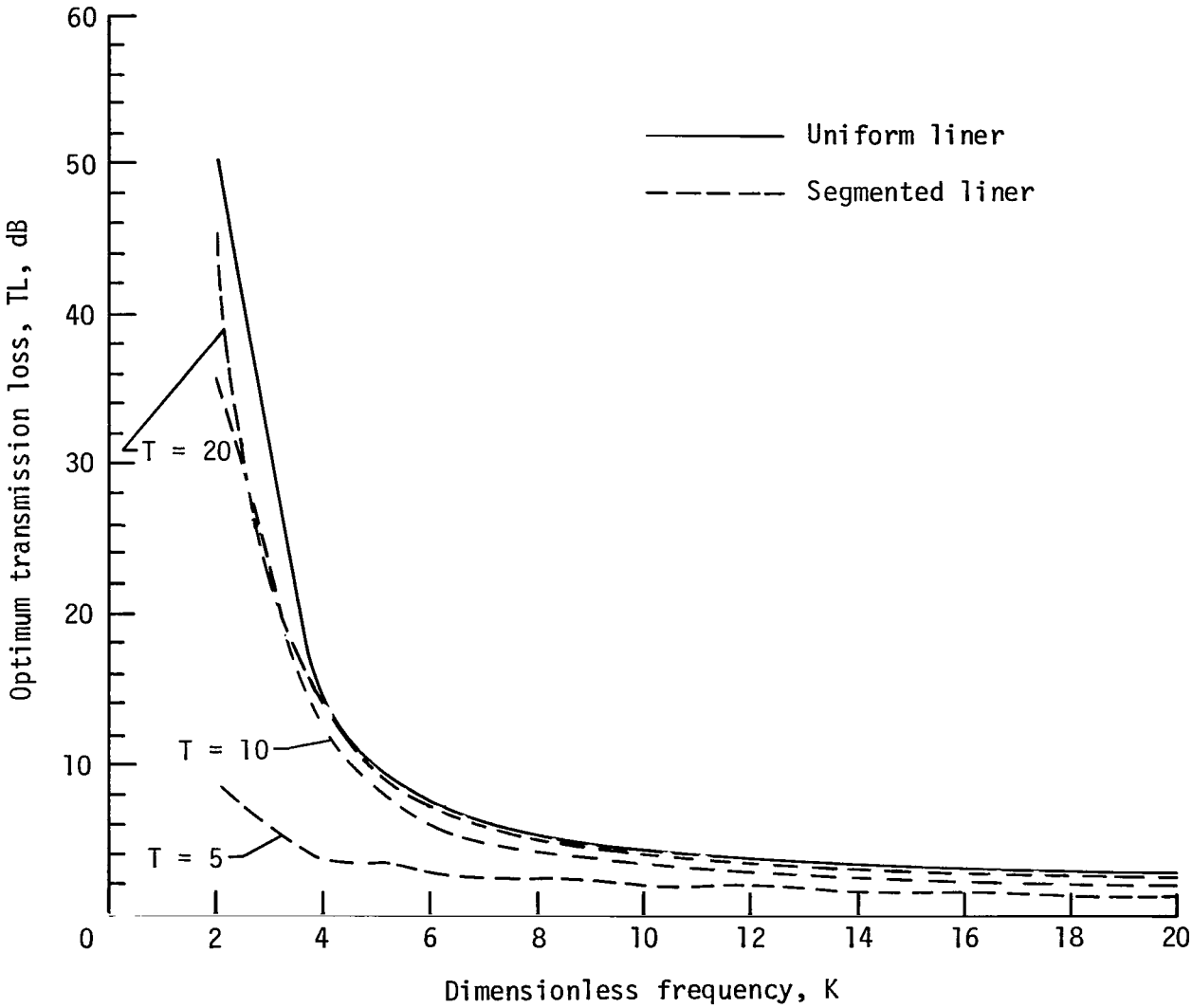

Figure 9.- Comparison of optimum transmission-loss spectrums for uniform and segmented liners for plane-wave source.

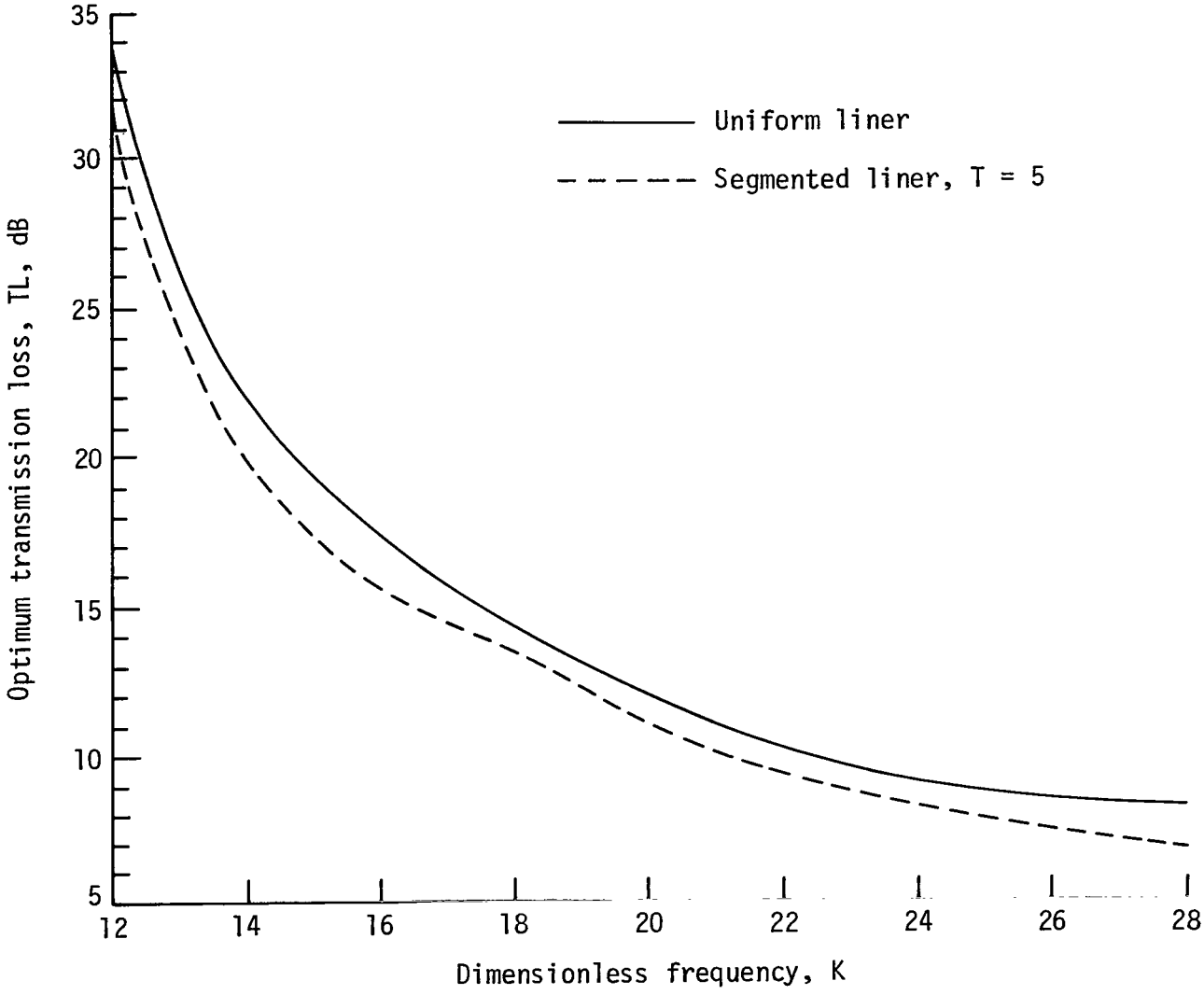

Figure 10.- Comparison of optimum transmission loss for standing-wave source. m = 5.

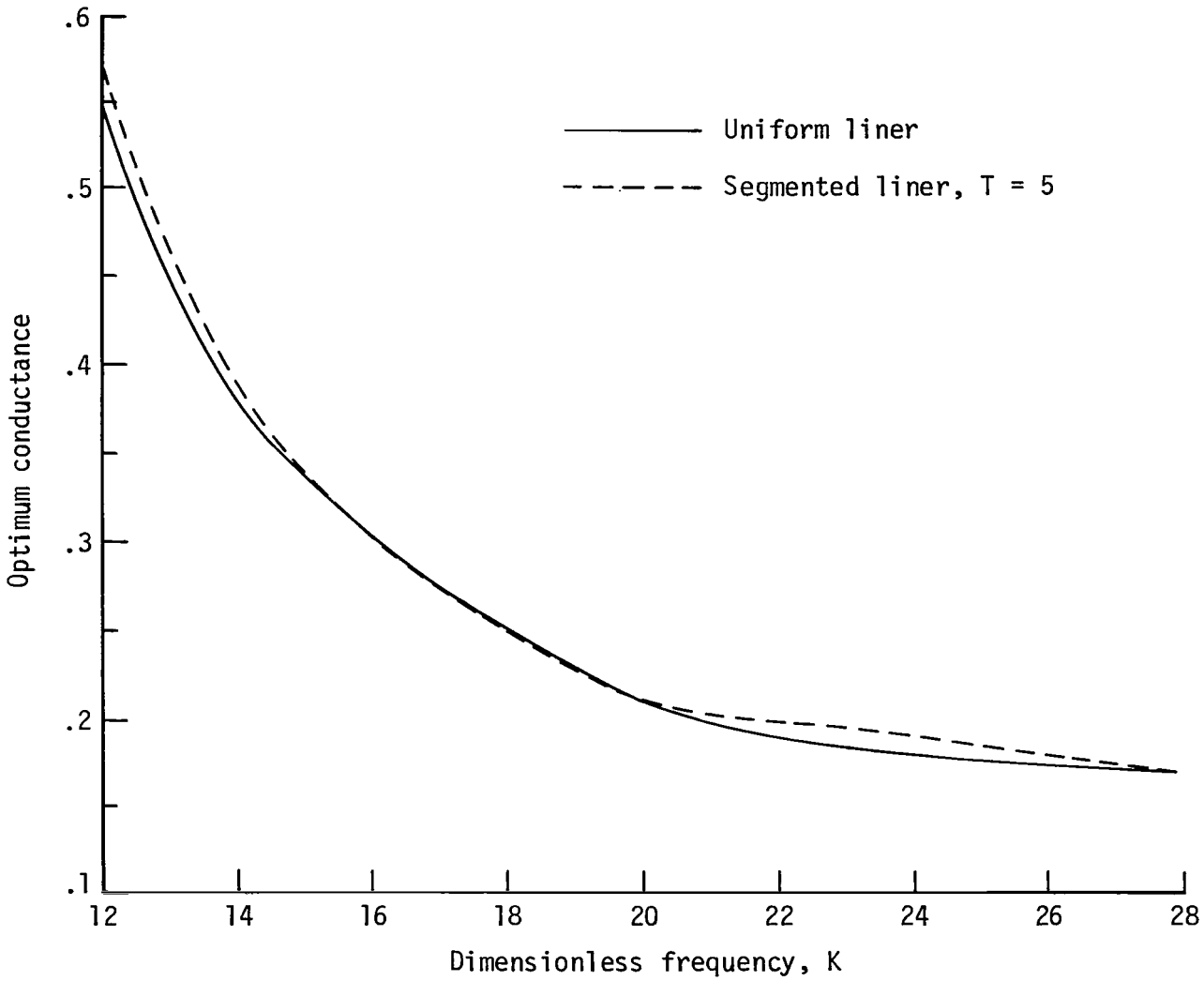

Figure 11.- Optimum conductance for standing-wave source. m = 5.

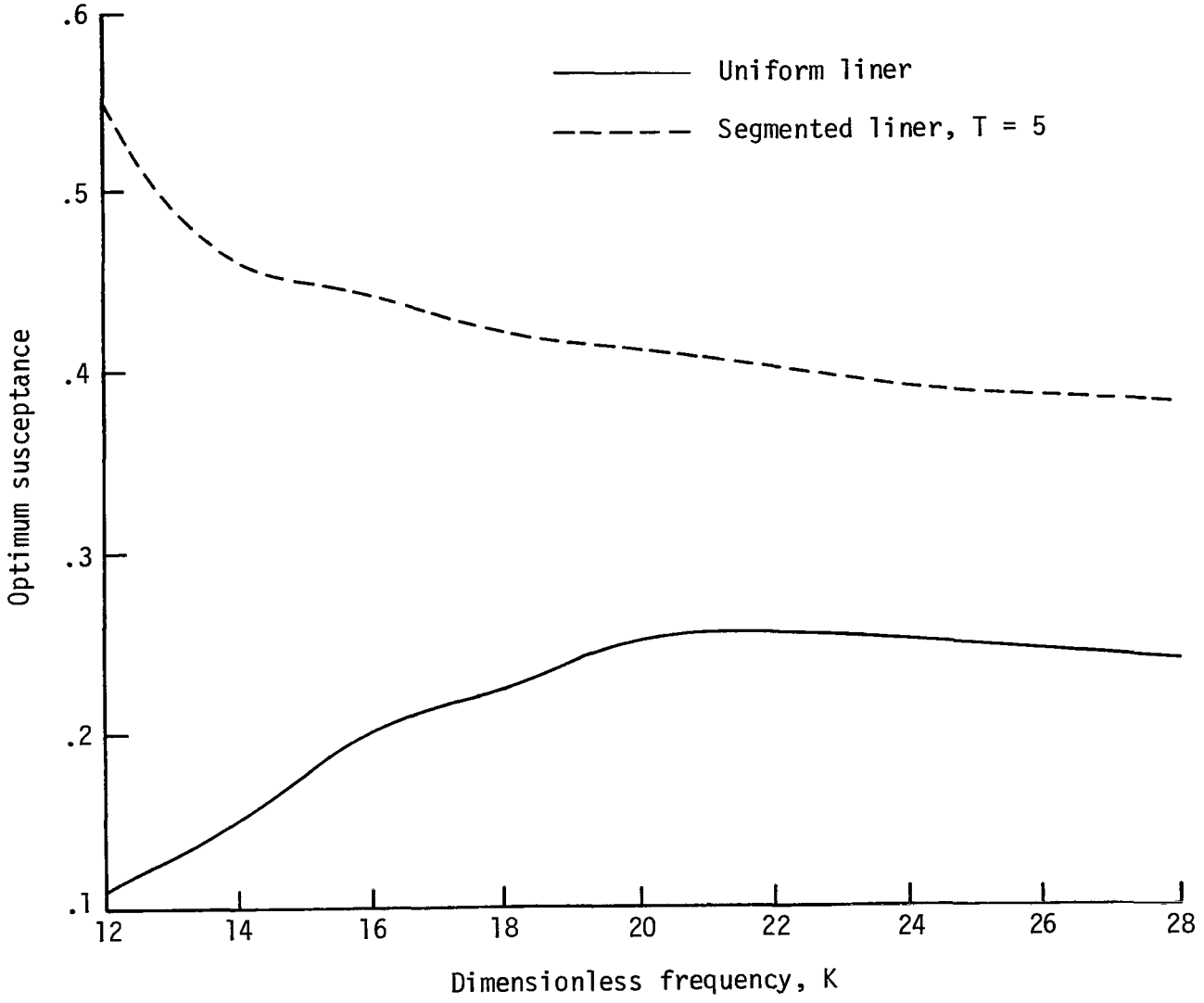

Figure 12.- Optimum susceptance for standing-wave source. m = 5.

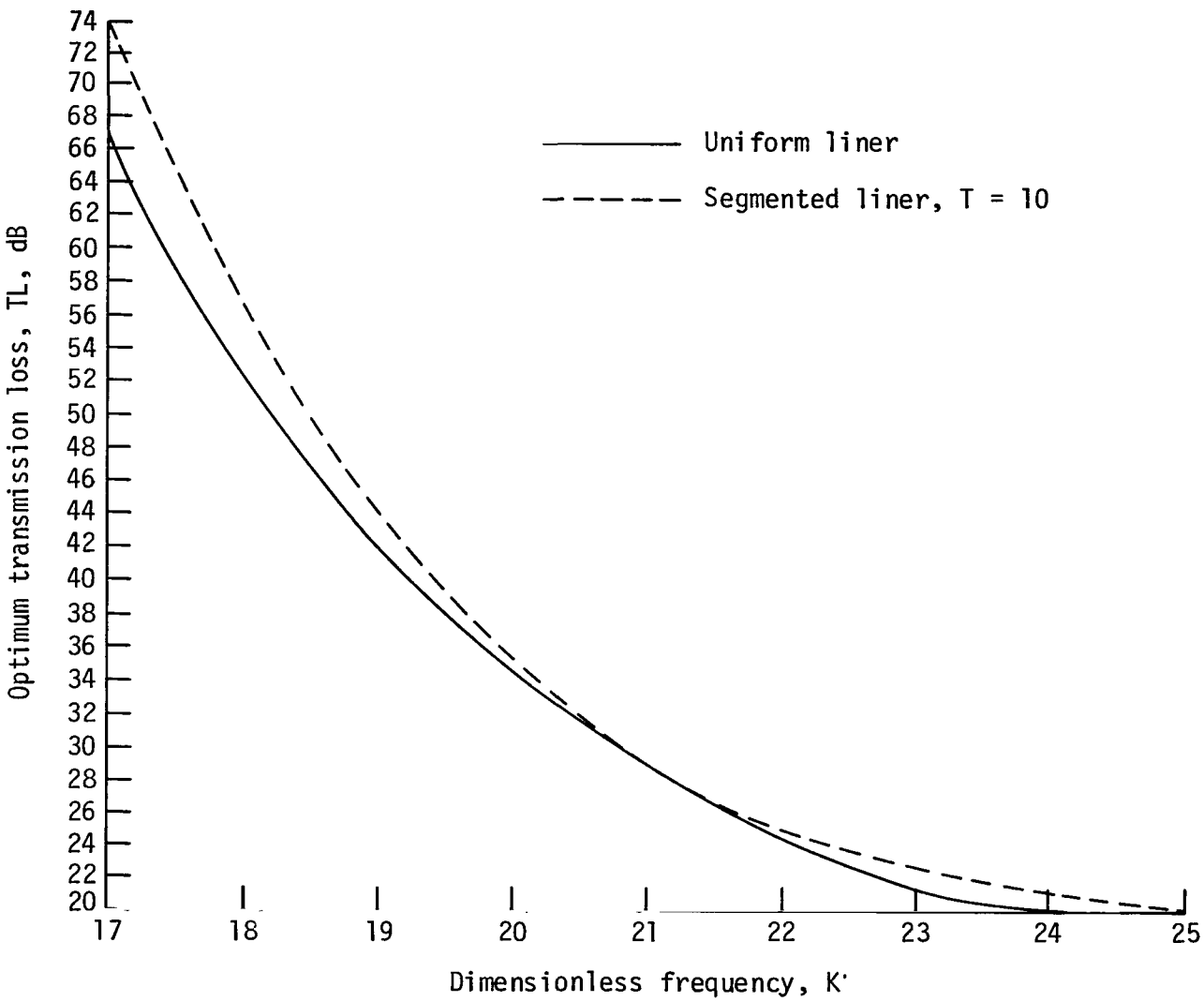

Figure 13.- Comparison of optimum transmission-loss spectrum for standing-wave source. m = 10.

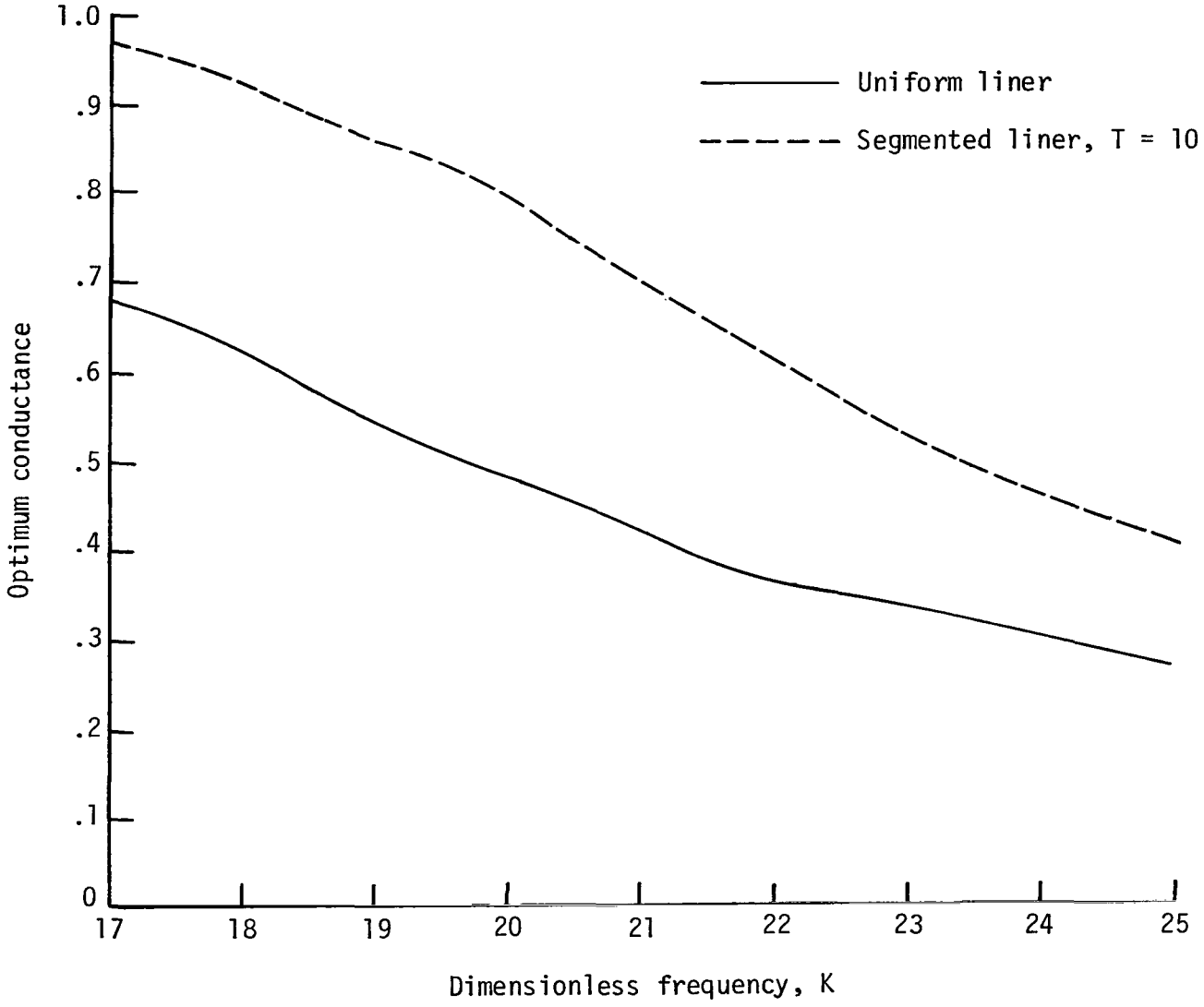

Figure 14.- Optimum conductance for standing-wave source. m = 10.

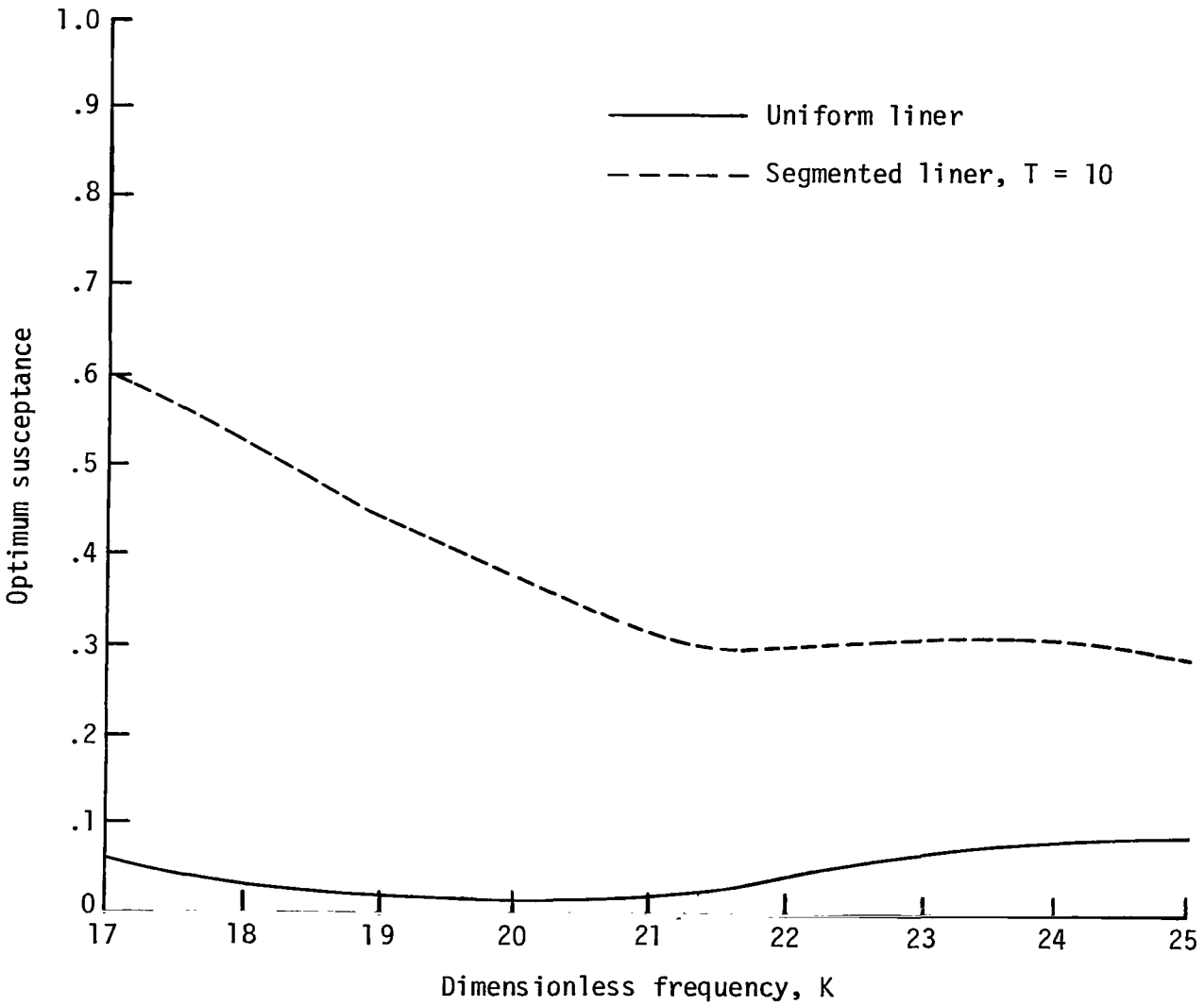

Figure 15.- Optimum susceptance for standing-wave source. m = 10.

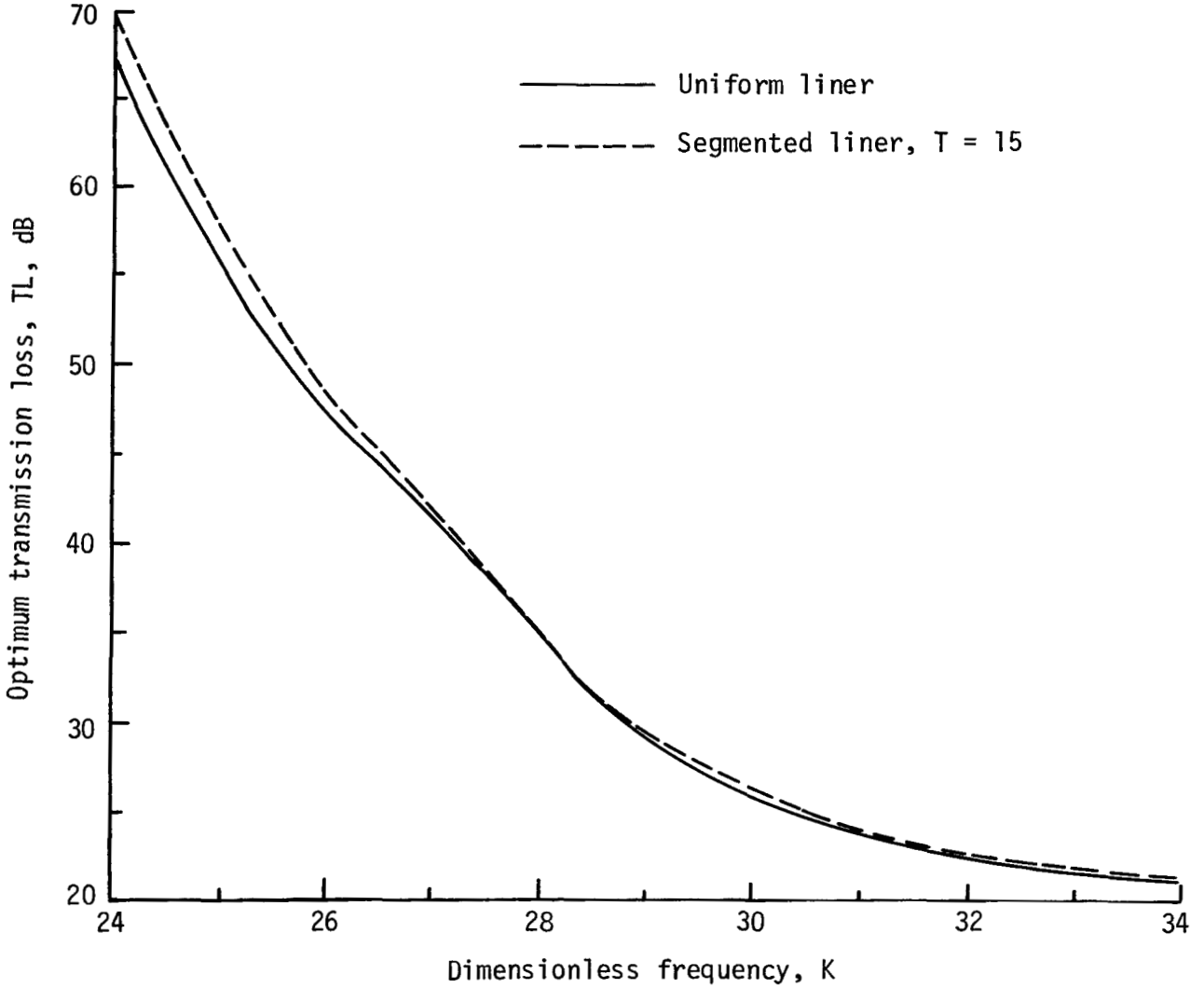

Figure 16.- Comparison of optimum transmission-loss spectrums for standing-wave source. m = 15.

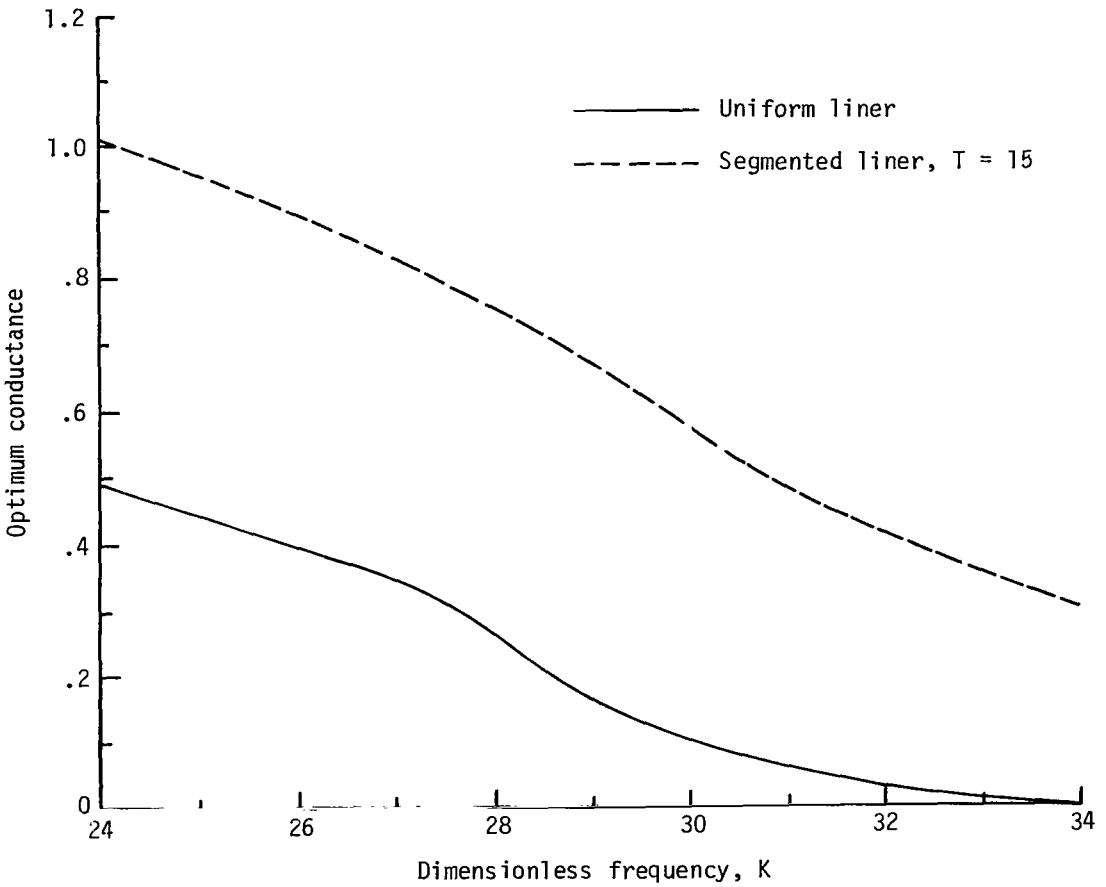

Figure 17.- Optimum conductance for standing-wave source. m = 15.

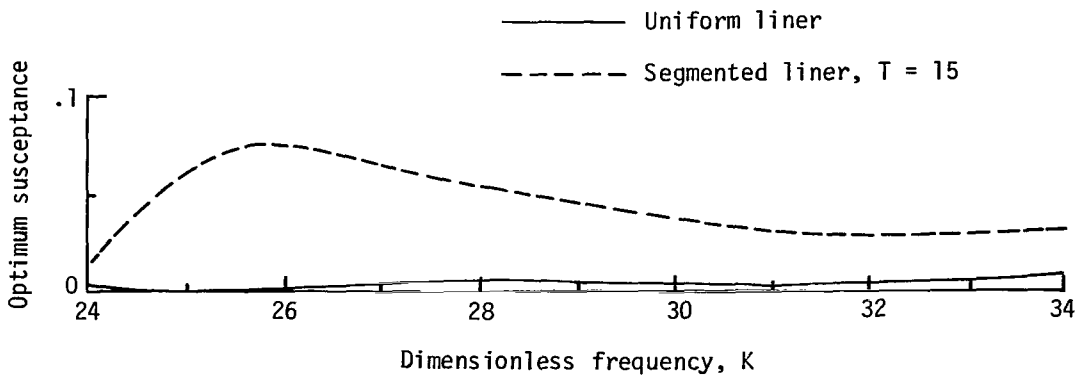

Figure 18.- Optimum susceptance for standing-wave source. m = 15.

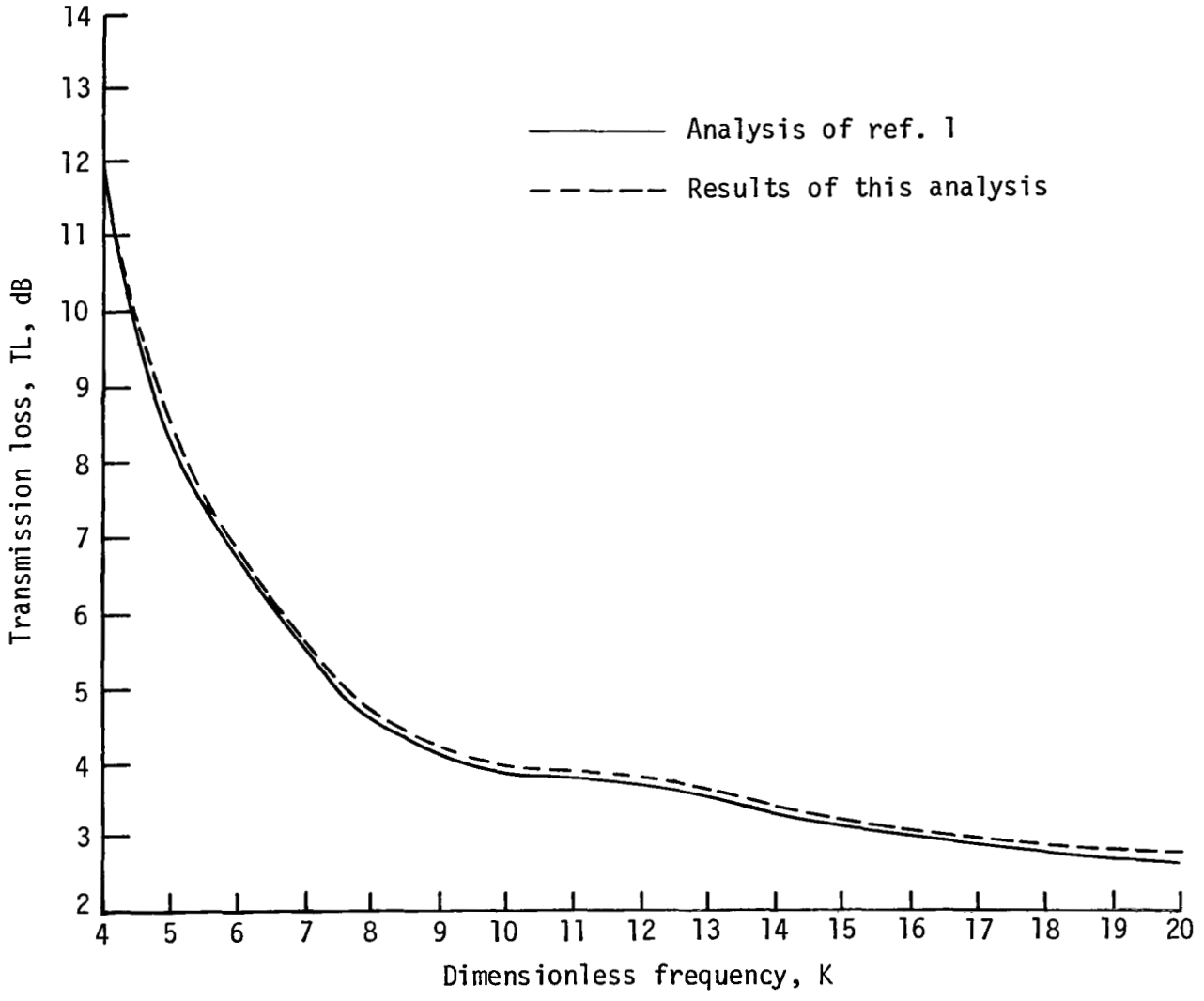

Figure 19.- Comparison of transmission losses predicted from two different analyses for plane-wave source.

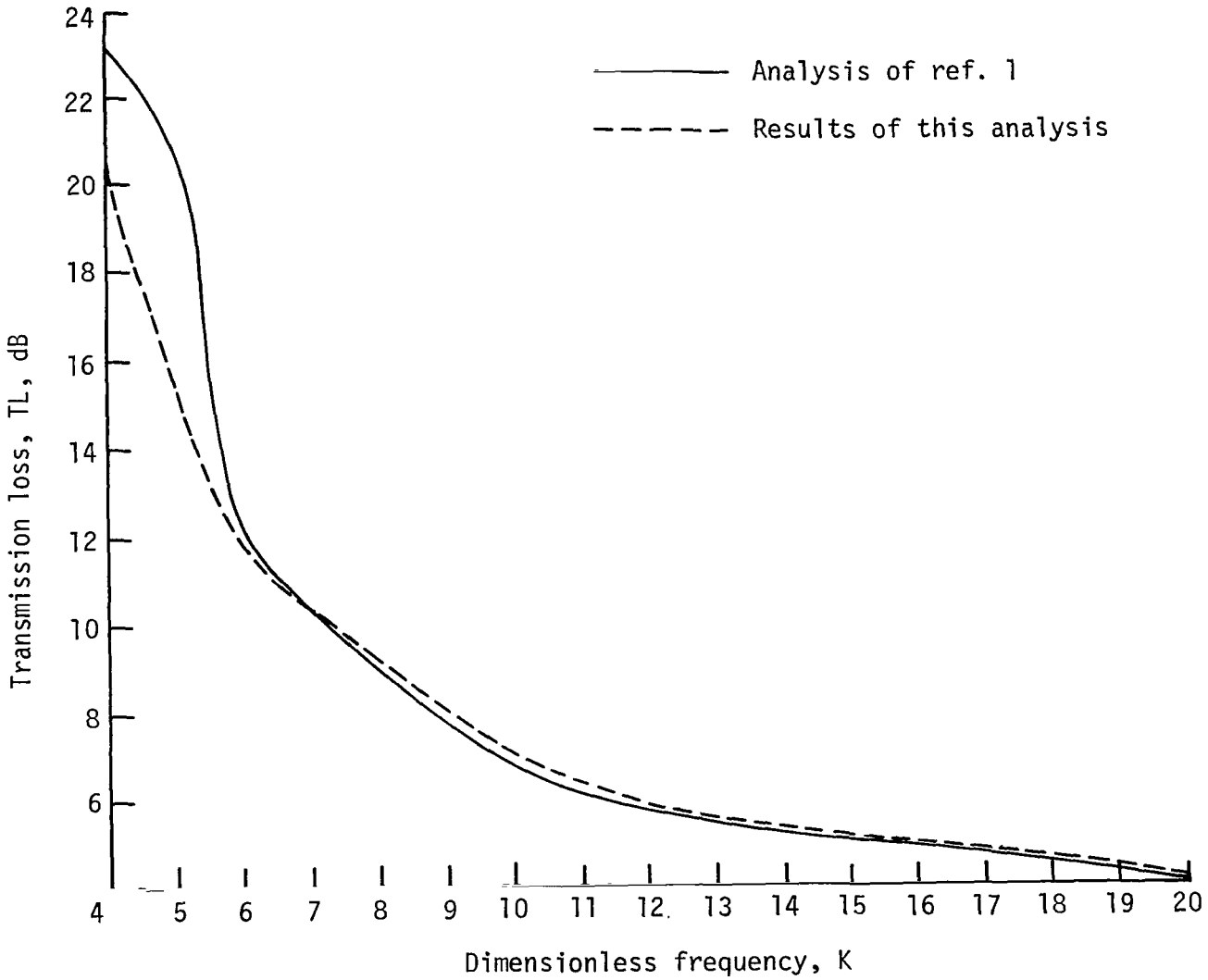

Figure 20.- Comparison of transmission losses predicted from two different analyses for standing-wave source. m = 1.

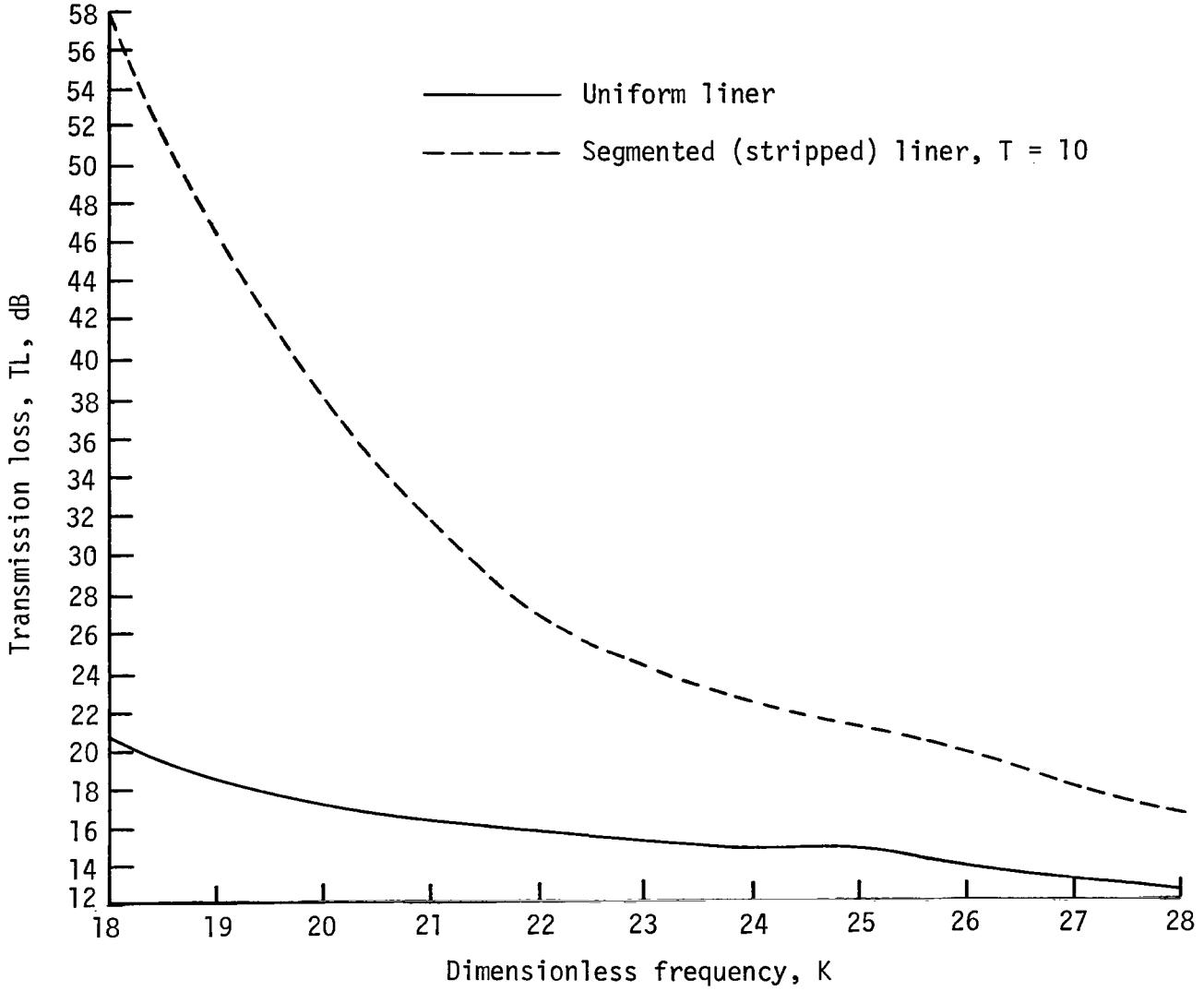

Figure 21.- Transmission loss of segmented (stripped) and uniform liners for standing-wave source. m = 10.

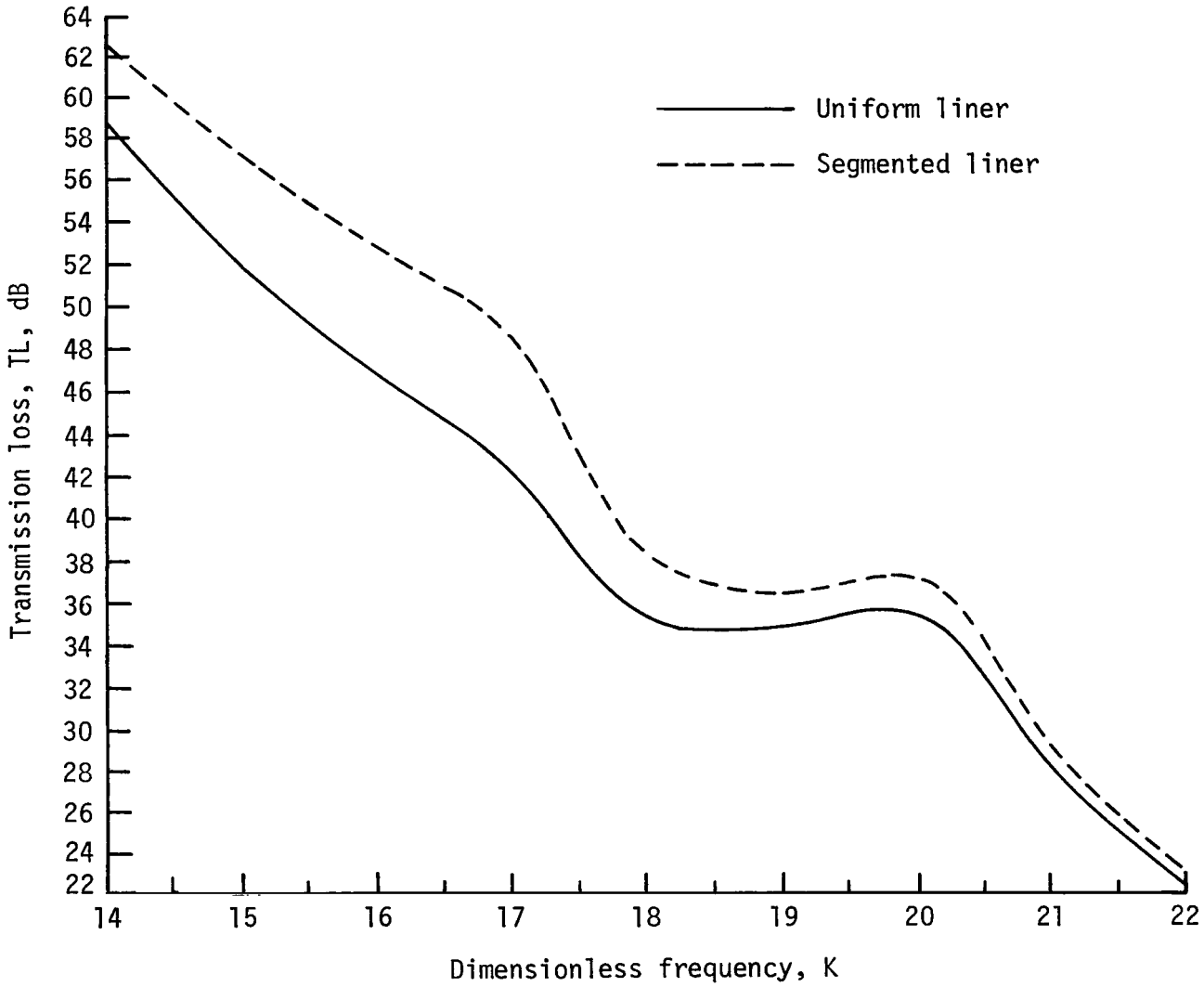

Figure 22.- Off-optimum performance properties for uniform and segmented liners tuned at K = 20.

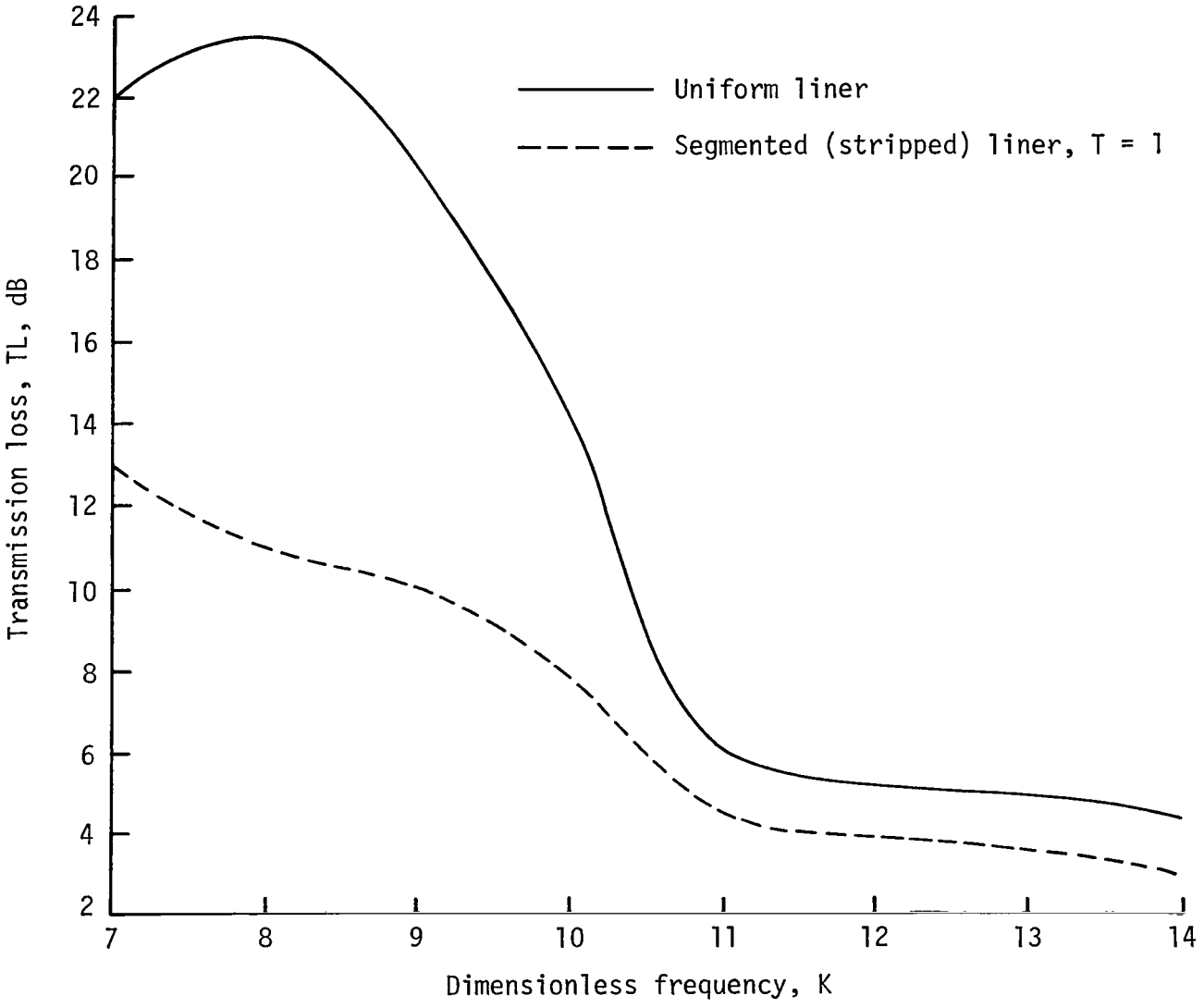

Figure 23.- Transmission-loss spectrums for uniform and segmented (stripped) liners for standing-wave source. m = 1; L = 1/2.

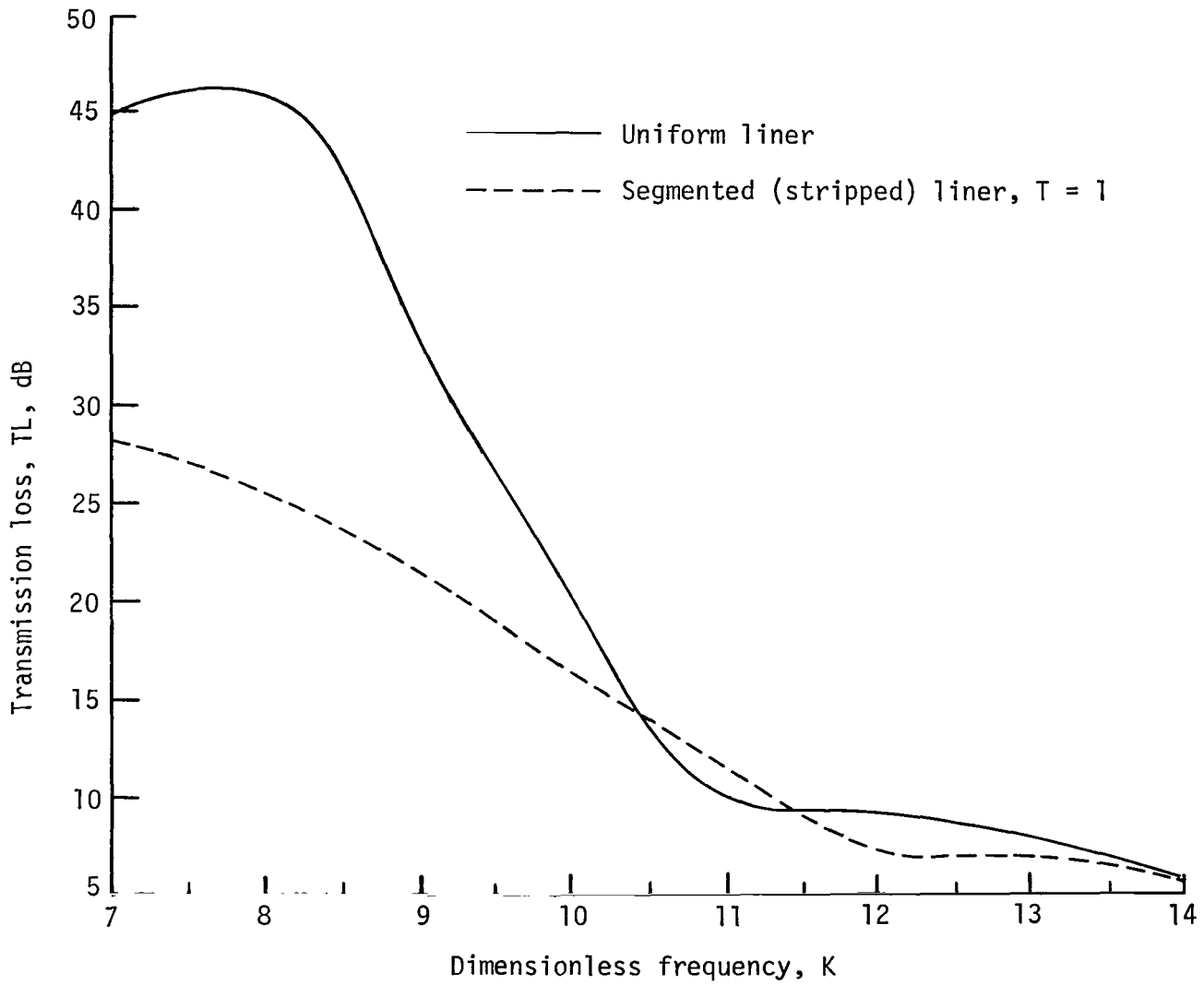

Figure 24.- Transmission-loss spectrum for uniform and segmented (stripped) liners for standing-wave source. m = 1; L = 1.

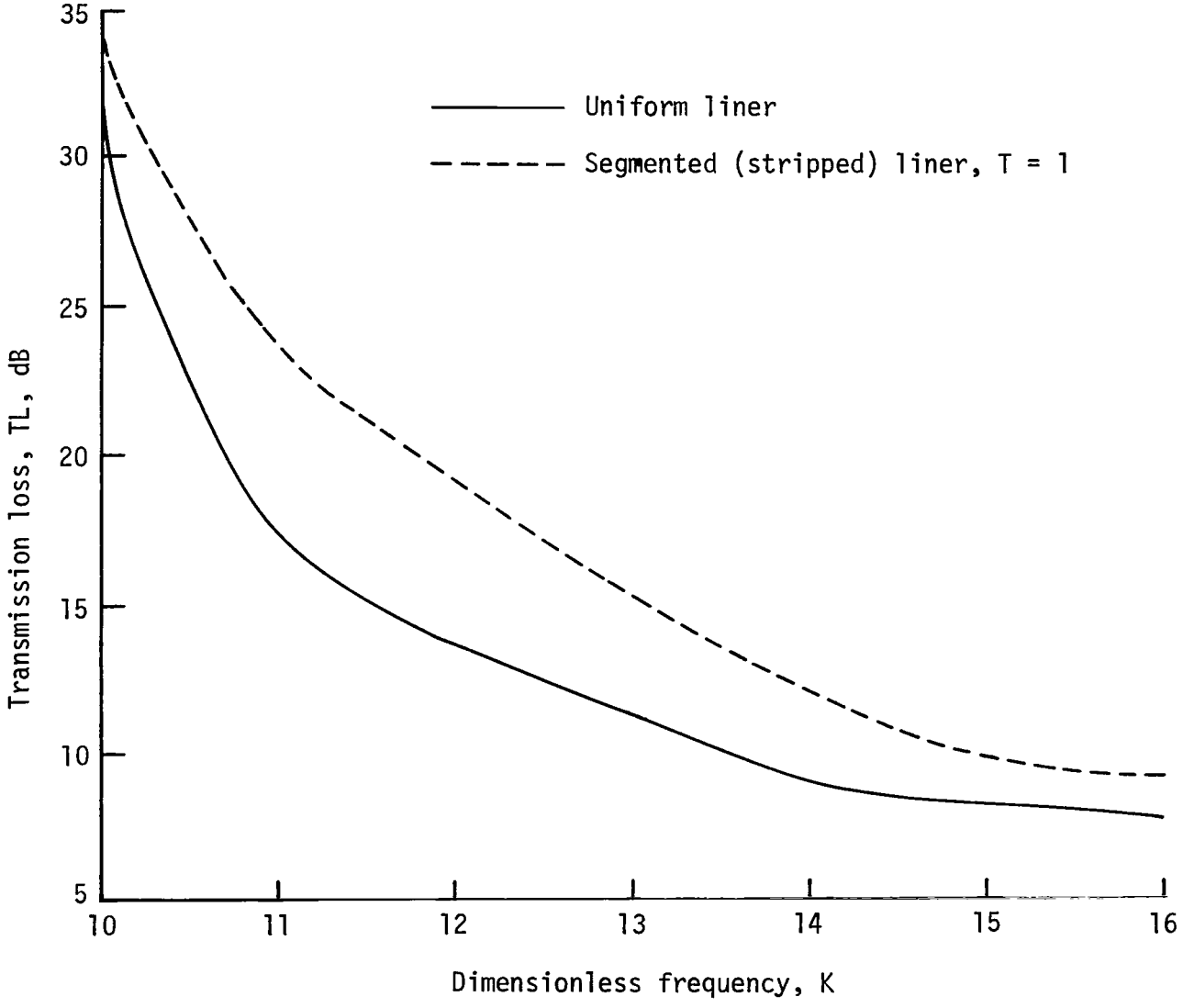

Figure 25.- Transmission-loss spectrum for uniform and segmented (stripped) liner for standing-wave source. m = 1; L = 2.

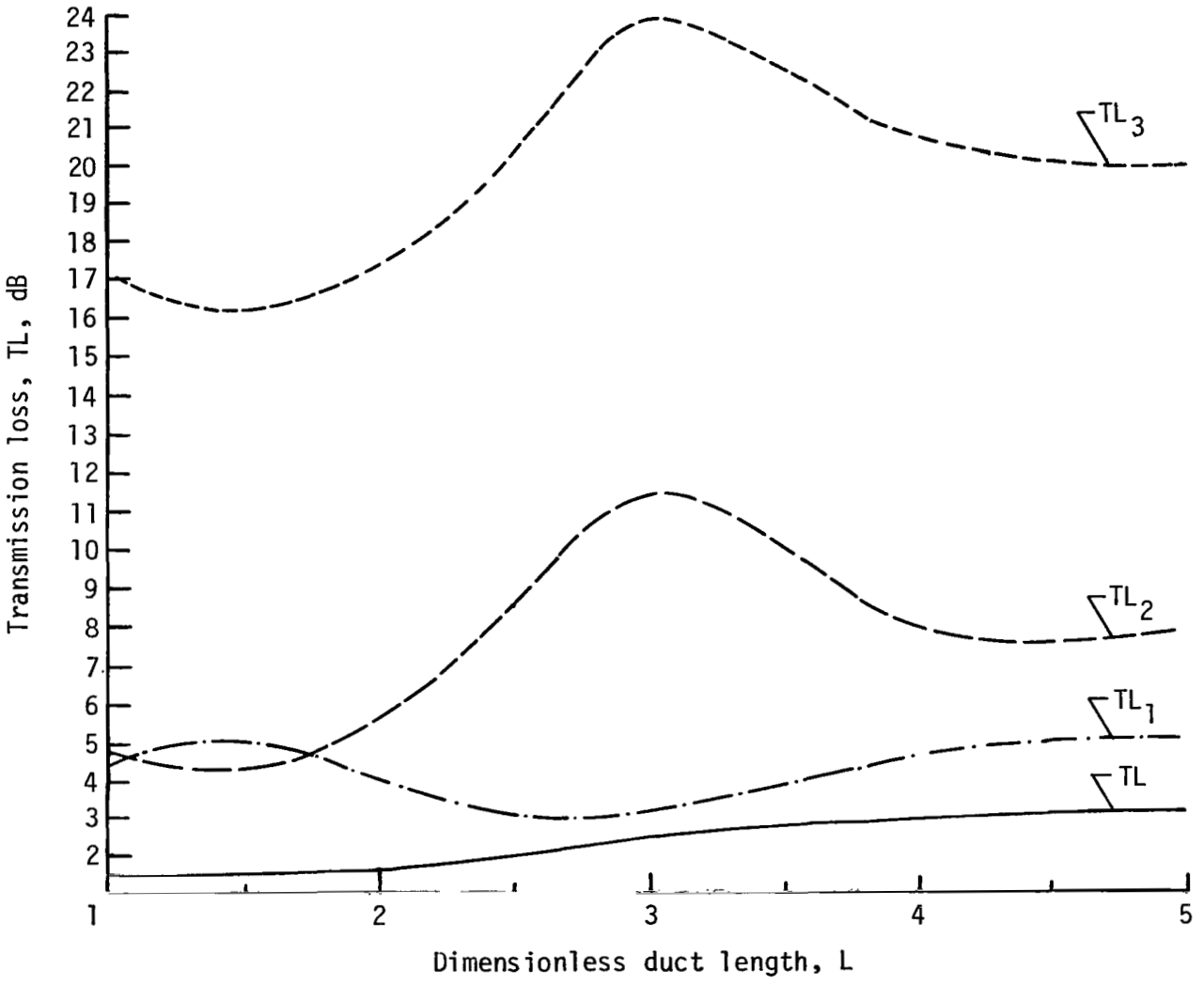

Figure 26.- Total and modal transmission losses for segmented liner with standing-wave source. m = 1.

1. Report No.	2. Government Accession No.	3. Recipient's Catalog No.
NASA TP-2075		

4. Title and Subtitle

CIRCUMFERENTIALLY SEGMENTED DUCT LINERS OPTIMIZED FOR AXISYMMETRIC AND STANDING-WAVE SOURCES

5. Report Date: September 1982

6. Performing Organization Code: 505-32-03-06

7. Author(s): Willie R. Watson

8. Performing Organization Report No.: L-15316

9. Performing Organization Name and Address

NASA Langley Research Center
Hampton, VA 23665

10. Work Unit No.

11. Contract or Grant No.

12. Sponsoring Agency Name and Address

National Aeronautics and Space Administration
Washington, DC 20546

13. Type of Report and Period Covered: Technical Paper

14. Sponsoring Agency Code

15. Supplementary Notes

16. Abstract

Optimum and off-optimum properties of circumferentially segmented duct liners are compared with those of uniform liners to identify any potential benefits of circumferential segmentation. Results are presented for both infinite and finite circumferentially segmented liners. High- and low-order spinning-mode sources are considered in the study. The solution for the segmented liner is obtained by a multimodal expansion of the segmented-liner eigenmodes in terms of a series of hard-wall duct modes. The coefficients in the hard-wall series are obtained by using Galerkin's method. Results show that for some frequencies and duct lengths, circumferentially segmented liners scatter energy equally between a higher and lower order circumferential wave number. Studies for higher order spinning-mode sources show that an optimized segmented liner with a hard-wall/soft-wall admittance variation representing an optimum configuration gives better performance than an optimized uniform liner. Overall, the greatest benefit of the segmented liner over the uniform liner occurs under off-optimum conditions. Also, the optimized segmented liner gives more effective broadband performance than the optimized uniform liner.

17. Key Words (Suggested by Author(s))

Circumferentially segmented liners
Variable-impedance boundary conditions
Global optimization technique
Galerkin method
Hard-wall duct mode expansion

18. Distribution Statement

Unclassified - Unlimited

Subject Category 71

19. Security Classif. (of this report)	20. Security Classif. (of this page)	21. No. of Pages	22. Price
Unclassified	Unclassified	48	A03

For sale by the National Technical Information Service, Springfield, Virginia 22161

NASA-Langley, 1982

2 1 1U,H, 820923 S00903DS
DEPT OF THE AIR FORCE
AF WEAPONS LABORATORY
ATTN: TECHNICAL LIBRARY (SUL)
KIRTLAND AFB NM 87117